1970

Annealing effects on the photoluminescence of gallium phosphide crystals

Donald Leroy Hughes
Lehigh University

ANNEALING EFFECTS ON THE PHOTOLUMINESCENCE OF GALLIUM PHOSPHIDE CRYSTALS

BY

Donald Leroy Hughes

ABSTRACT

Zinc and oxygen doped gallium phosphide crystals were solution grown at 1170°C. Debye-Scherrer film and Laue patterns indicated that GaP single crystals were grown with the face parallel to a (111) plane. Resistivity and Hall effect measurements were made from which carrier concentrations and mobilities were calculated.

Effects of annealing were studied as a function of time at 400°C and at 600°C. After every annealing cycle photoluminescent efficiency and photoluminescent spectra measurements were made. The observed shifting of emission from the infra-red to red with annealing time corroborated earlier experimental work done by Onton and Lorenz by electroluminescent studies. Variations in red to infra-red intensity ratios with annealing time and temperature were related to a theoretical paired-defect model.

The results substantiated a proposed model that red emission is due to exciton Zn-O complex recombination and that infra-red emission is due to an ionized oxygen to an ionized zinc recombination. In order to explain the experimental results related to total quantum efficiency, two other models were proposed. First, since it was observed that there is a higher photoluminescent efficiency for lower annealing temperatures, it was proposed that the exciton Zn-O complex recombination is more probable than the ionized donor to ionized acceptor recombination. Second, it was proposed that some interstitial oxygen diffuses to substitutional sites which

explains why the "t=0 condition" can be reset for equilibrium Zn-O complexes, but cannot be reset for external quantum efficiency.

ANNEALING EFFECTS ON THE PHOTOLUMINESCENCE OF GALLIUM PHOSPHIDE CRYSTALS

BY
Donald Leroy Hughes

ABSTRACT

Zinc and oxygen doped gallium phosphide crystals were solution grown at 1170°C. Debye-Scherrer film and Laue patterns indicated that GaP single crystals were grown with the face parallel to a (111) plane. Resistivity and Hall effect measurements were made from which carrier concentrations and mobilities were calculated.

Effects of annealing were studied as a function of time at 400°C and at 600°C. After every annealing cycle photoluminescent efficiency and photoluminescent spectra measurements were made. The observed shifting of emission from the infra-red to red with annealing time corroborated earlier experimental work done by Onton and Lorenz by electroluminescent studies. Variations in red to infra-red intensity ratios with annealing time and temperature were related to a theoretical paired-defect model.

The results substantiated a proposed model that red emission is due to exciton Zn-O complex recombination and that infra-red emission is due to an ionized oxygen to an ionized zinc recombination. In order to explain the experimental results related to total quantum efficiency, two other models were proposed. First, since it was observed that there is a higher photoluminescent efficiency for lower annealing temperatures, it was proposed that the exciton Zn-O complex recombination is more probable than the ionized donor to ionized acceptor recombination. Second, it was proposed that some interstitial oxygen diffuses to substitutional sites which

ANNEALING EFFECTS ON THE PHOTOLUMINESCENCE OF GALLIUM PHOSPHIDE CRYSTALS

by

Donald Leroy Hughes

A Thesis

Presented to the Graduate Committee

of Lehigh University

in Candidacy for the Degree of

Master of Science

in Metallurgy and Materials Science

Lehigh University

1970

CERTIFICATE OF APPROVAL

This thesis is accepted and approved in partial fulfillment of the requirements for the degree of Master of Science.

May 13, 1970
Date

Michael R. Notis 5/13/70
Professor in Charge

G. P. Girard
Chairman of the Department
of Metallurgy and Materials
Science

ACKNOWLEDGEMENTS

The author wishes to express sincere appreciaton to Dr. M. R. Notis of Lehigh University for his guidance during the course of this investigation and for helpful suggestions in the preparation of the text. Sincere appreciation is also expressed to the Western Electric Company for sponsoring the graduate studies of which this thesis is a part. Grateful acknowledgement is extended to Dr. H. D. Pruett of Western Electric for his guidance during the course of this investigation, including the design of the photon counting equipment and aid in setting up related equipment that was used in the investigation, and for helpful suggestions in the preparation of the text. Acknowledgement is extended to the following members of the Western Electric Company: J. M. Donohue of the GaP Measurements Laboratory, A. K. Lagarde, Research Leader, K. L. Morton of the Analytical Laboratory, and M. J. Lim of the GaP Crystal Growing Laboratory. Appreciation is extended to the following members of Bell Telephone Laboratories: L. Derrick and F. Trumbore for assistance and discussions on crystal growing, J. Jayson for providing equipment for Hall and resistivity measurements as well as valuable discussions on mechanisms of light emitting diodes, J. D. Wiley for his discussion of the theoretical development of pair formation, and W. Erdman for sputtering the SiO_2 thin film.

Above all, the author is deeply indebted to his wife, Mrs. Betty Jean Hughes and his children, Donnie and Rebecca, with whose understanding and appreciation this work would not have been possible.

TABLE OF CONTENTS

LIST OF TABLES

LIST OF FIGURES

ABSTRACT

Zinc and oxygen doped gallium phosphide crystals were solution grown at 1170°C. Debye-Scherrer film and Laue patterns indicated that GaP single crystals were grown with the face parallel to a (111) plane. Resistivity and Hall effect measurements were made from which carrier concentrations and mobilities were calculated.

Effects of annealing were studied as a function of time at 400°C and at 600°C. After every annealing cycle photoluminescent efficiency and photoluminescent spectra measurements were made. The observed shifting of emission from the infra-red to red with annealing time corroborated earlier experimental work done by Onton and Lorenz by electroluminescent studies. Variations in red to infra-red intensity ratios with annealing time and temperature were related to a theoretical paired-defect model.

The results substantiated a proposed model that red emission is due to exciton Zn-O complex recombination and that infra-red emission is due to an ionized oxygen to an ionized zinc recombination. In order to explain the experimental results related to total quantum efficiency, two other models were proposed. First, since it was observed that there is a higher photoluminescent efficiency for lower annealing temperatures, it was proposed that the exciton Zn-O complex recombination is more probable than the ionized donor to ionized acceptor recombination. Second, it was proposed that some interstitial oxygen diffuses to substitutional sites which

explains why the "t=0 condition" can be reset for equilibrium Zn-O complexes, but cannot be reset for external quantum efficiency.

I INTRODUCTION AND PURPOSE

It is possible for solids to generate visible light in several ways. A solid can be raised to a sufficiently high temperature to emit light, as in the case of a tungsten incandescent lamp; or electrical energy can be converted directly into light by luminescence [1]. In 1923 Lossev [2] applied a direct current to a SiC semiconductor crystal to generate visible light. In 1937 G. Destriau [3] of France generated light by applying an alternating voltage to an insulator containing luminescent powder. An example of this type of luminescence is the faintly-glowing green night lights that plugs into the household outlet [1]. Still later, in 1952, studies were made on electroluminescence of p-n junctions of germanium. Due to extremely low efficiencies of converting electrical current to photons, little interest was aroused [4]. By 1962 it was found that GaAs had a higher conversion efficiency in the infra-red region [5]. At about the same time the use of $GaAs_{1-x}P_x$ led, at low temperatures, to laser action which was visible to the eye [6]. A little later a GaP red light emitting diode was reported which emitted non coherent radiation at $300^{\circ}K$ with an external quantum efficiency of about 1.5 per cent [7].

There are several ways of exciting carriers to obtain luminescence in a solid crystal. All of the ways that will be discussed involve the creation of a large number of electron-hole pairs per unit volume. Excitation can be by irradiation with photons (photoluminescence),

or electrons (cathodoluminescence), or by minority carrier injection in a forward biased p-n junction (electroluminescence). In all cases, after excitation the excess carriers may recombine radiatively to emit light if the band gap is in the visible portion of the spectrum [8-9].

In photoluminescence the exciting photon energy must be greater than the band gap in order to create a hole-electron pair. This technique allows one to obtain information about the luminescent processes. Both qualitative and quantitative information can be obtained about the material without making p-n junctions. It is possible to obtain high injection levels by a mercury lamp [8-9] or by an Argon laser [10-11].

Recombination of carriers may occur in a variety of ways (Figure 1). There can be a direct recombination of electrons and holes (Figure 1a) or there can be recombination through intermediate states (Figures 1b-1d). The various processes are competetive but can be analyzed by Shockley-Read-Hall statistics [12-13]. If the hole and the electron have the same momentum in E-k space, a direct transition (Figure 2a) can occur, but if the hole and electron do not have the same momentum, an indirect transition which involves the absorption or emission of a phonon is required to conserve momentum (Figure 2b).

In order for an electroluminescent diode to be of use for visual display purposes there are two conditions which must be satisfied[1,14]

First, some, or all of the band gap energy of an electron injected into the conduction band must be given up by photon emission rather than by direct lattice interactions. Second, the band gap of the diode must be large, 1.75 eV or more, so that the photons which are generated fall in the visible region of the spectrum. The problem that arises is to satisfy both of the above conditions. Since radiative recombination is possible in a direct band-gap material, this material is sometimes more efficient. Gallium arsenide, a direct transition material that is very efficient, emits in the infra-red region. Many ternary compounds have large enough direct gap transitions, but reproducibility in growing the crystal is difficult. Gallium phosphide has a large energy gap, but, because it is an indirect band-gap material, it must be judiciously doped to produce reasonably efficient radiative recombination [15].

Originally it was thought by Gershenzen, et al [16-17] and Nelson [18] that red luminescence of GaP could be attributed to donor-acceptor pair recombination ("donor-acceptor pair luminescence" Figure 3a). However, now it is understood that the oxygen deep donor traps an electron and the shallow zinc acceptor traps a hole, and when the two recombine, a photon is given off with energy in the infra-red region. Later evidence shows that red luminescence results from either the decay of an exciton bound to a nearest neighbor Zn-O complex ("exciton luminescence" Figure 3b), or the recombination of electrons bound to neutral Zn-O complexes with holes trapped at distant Zn acceptors [19-20] ("pair luminescence," Figure 3c). A bound exciton is formed by a two-step process in

which a neutral Zn-O complex first traps an electron. After the electron is trapped, the now-negative Zn-O complex can attract a hole through a coulombic force. When the force is sufficiently strong to actually bind a hole, an exciton is formed which is bound at the site of the Zn-O complex. Since the bound exciton represents an excited state, it can decay radiatively to produce the so-called "bound-exciton emission band." If a bound exciton is not formed, the electron trapped at the Zn-O complex may eventually radiatively recombine with a hole trapped at a distant zinc acceptor site to produce pair recombination.

The pair recombination between electrons trapped at Zn-O complexes with holes trapped at distant zinc acceptors will produce visible light. The second type of pair recombination results from electrons at the deep-donor oxygen sites recombining with holes at the shallow acceptor zinc sites to produce infra-red radiation.

It is possible to distinguish "pair luminescence" from "exciton luminescence" by observing the weak vibrational sidebands of the latter. At a temperature below 70°K pair luminescence dominates [10,21] but above 70°K to room temperature exciton luminescence dominates [21]. If the electron-hole recombination energy were given to a third particle, a nonradiative or Auger recombination would occur. Low efficiency results from any transition that does not produce light.

There are several ways of defining the efficiency of emission in GaP [15]. First, the external power efficiency is defined as

$$(\eta_p)_{ext} = \frac{\text{optical power out}}{\text{electrical power in}} \quad . \qquad (1)$$

External power efficiency is related to internal power efficiency by the equation

$$(\eta_p)_{int} = (\eta_p)_{ext} \, F \qquad (2)$$

where F is a correction factor which accounts for all internal absorption. Although GaP is not highly absorbing of its own red luminescence, its high refractive index ($\delta = 3.5$) prevents the escape of radiation beyond a 17° cone. That is, light striking the surface at an angle greater than 17° with respect to the normal is totally reflected. Some of the totally reflected light eventually escapes but the effect of multiple internal reflections is to greatly increase the path length in the crystal and, hence, to increase the probability of internal absorption. Another way of defining the efficiency of emission of GaP is by the external quantum efficiency which is defined as

$$(\eta)_{ext} = \frac{\text{photons out}}{\text{photons in}} \qquad (3)$$

The external quantum efficiency can be related to internal quantum efficiency in the same manner as the power efficiency.

A method of measuring efficiency is to line a cavity with solar cells to absorb the light emitted by the material. The panels of solar cells generate an electrical signal proportional to the amount of light emitted by the sample under test. It is necessary to

calibrate the solar cell panel using a known light source. Details of the equipment will be discussed in section III.

Another important parameter to consider is the luminous efficiency which is a measure of the response of the eye to the frequency of the emitted radiation for a given power output [15] (Figure 4). The luminous efficiency can be calculated from the following equation:

$$\eta_L = \frac{P_{opt}\,\phi}{I_D} \tag{4}$$

where ϕ is the luminous conversion factor in lumens/watt for the light output of a given type of light emitting diode, P_{opt} is the optical power out in watts and I_K is the diode current in amperes. Sometimes another definition is used for the luminous efficiency. Denoting the second definition by η_L' (in lumen per watt), it is related to the first definition by,

$$\eta_L' = \frac{\eta_L}{V_D} \tag{5}$$

where V_D is the bias voltage on the light emitting diodes. For example, green light may have a quantum efficiency 40 times smaller than red light and still be just as bright to the eye. Light emitting diodes have been produced with external quantum efficiencies of .1% for green light [22] and 2% for red light [23].

Several studies have indicated that heat treatment can improve the visible light output of electroluminescent GaP diodes by as

much as an order of magnitude [22-23]. Onton and Lorenz [24] have shown that there is a relationship between the visible peak at 1.80 ev and the infra-red peak at 1.37 ev. By various heat treatments they were able to shift the intensity of emission from the visible red to the infra-red. They indicate that the red 1.80 ev peak corresponds to bound exciton decay while the 1.37 ev infra-red peak corresponds to ionized donor to ionized acceptor pair recombination. By heat treating GaP at high temperatures, Zn-O nearest neighbor pairs are dissociated, and the ionized oxygen donor concentration is accordingly increased. Since oxygen that is not in a Zn-O complex can participate in ionized-pair recombination, the infra-red emission efficiency is increased at the expense of the visible emission efficiency. Conversely, low temperature heat treatment increases the formation of nearest neighbor Zn-O pairs which improves red emission.

In an early model, Maeda [25] explained the dependence of efficiency on heat treatment by conventional donor-acceptor pair recombination. In later work by Maeda, et al [26], they found annealing increases visible emission by a factor of 20 to 50 and decreases the current density from 1/3 to 1/6 that of quenched diodes. They attribute the decrease in current density to annihilation of deep recombination centers in the depletion layer. The increase in emission intensity is described as being due to an increase in the lifetime of minority carriers and an increase in the relative intensity of red to infra-red emission [26-27].

The purpose of this investigation is to show that part of the increase in efficiency in the visible region due to annealing can be attributed to the shift in emission from the infra-red peak to the red peak. If part of the Zn-O nearest neighbor complexes could be broken up by high temperature treatment, the ratio of red to infra-red energy would be lower. By annealing at low temperatures part of these Zn-O complexes would reform and the ratio would be much greater. The lower the temperature the greater the ratio would be after the equilibrium number of pairs had been reached.

It was decided that photoluminescent studies made on p type material would provide a more basic understanding of the mechanism involved in recombination than the previous work involving electroluminescent diodes. In addition, it would not be necessary to become involved in any geometric considerations that would be essential if diodes were studied.

II CRYSTAL GROWTH, SAMPLE PREPARATION AND ANNEALING

A Marshall combustion tube furnace, model #1147, which has a resistive load, was used to grow the GaP single crystals. The mullite combustion tube was 24 inches long and 3 inches in diameter. The furnace has posts that permit resistance wire shunting to obtain the profile desired.

Due to the critical nature of the temperature control, a Leeds and Northrup (L&N) controller package with a Silicon Controlled Rectifier was used. The resulting temperature variation was less than $1/2^{\circ}C$ in the center of the combustion tube. The crystal growing equipment is shown in Figure 5.

In order to profile the furnace along its length a syncronous motor with different gear ratios for attaining variable speed control was connected to a worm gear with a thermocouple on the end. Figure 6 shows the profile for crystal growth.

The actual temperature of the furnace during crystal growth was monitored by five Pt/Pt-10% Rhodium thermocouples which were connected to an L and N Speedomax W strip chart recorder. This recorder could receive and plot multiple input signals simultaneously. Each of the five thermocouples was placed at 1 inch increments up from the bottom of the crystal growth ampoule (Figure 5) with the thermocouple placements numbered 1,2,3,4, and 5. Since the profile plot is shown in Figure 6 and the gradient had the same form for all the thermocouples, only one plot of temperature (thermocouple #5) versus time is shown in Figure 7.

A Varian Vac-Sorb pump, model #941-6001 was used for rough pumping to 10 microns, and then a Varian Vac-Ion pump, model #911-5011 was used for final pumping to 10^{-8} torr. Due to the length of the tubing from the vacuum system to the ampoule, the actual pressure was estimated to be approximately 10^{-6} torr. As shown in Figure 5, two inlet valves, A and B were used for purging with nitrogen and hydrogen respectively, and a Cajon ultra-torr* glass to metal fitting was used for connecting the ampoule to the vacuum station.

Before the crystals were grown the ampoule was cleaned thoroughly with trichloroethylene, methanol, hydrofluoric acid and deionized water (see Appendix A). After the cleaning procedure, .07 mole % Zn** and .04 mole % Ga_2O_3 were loaded into the arm of the ampoule to prevent volatization of the dopants during bake out of the ampoule (Figure 5 and Figure 8). These doping concentrations were found to be optimum when the crystals were grown [23,28]. Ninety weight % Ga and 10 weight % polycrystalline GaP were added to the bottom of the ampoule. This ratio was determined from the Ga-GaP phase equilibrium diagram and gives a liquidus temperature of 1100°C [29]. If a higher temperature were used, silicon contamination from the ampoule might become a problem; alternatively, if a lower temperature were used, the amount of GaP would be so low that only small crystals would be grown [30].

---

* The Cajon ultra-torr fitting was purchased from Penn Valve & Fitting Company.

** The suppliers and purities of the raw material is presented in section IV.

The ampoule was connected to the vacuum station by the ultra-torr fitting shown in Figure 5. After pumping down to 10^{-6} torr, the ampoule was back filled with ultra high purity N_2* through valve A to atmospheric pressure. The system was pumped down a second time to 10^{-6} torr and was then backfilled with ultra high purity H_2 to one atmosphere through valve B. The ampoule was placed into the Marshall furnace in the bake out position shown in Figure 5 and baked out at 900°C for 10 minutes [30]. (Care was taken to prevent the arm of the ampoule from rising above 50°C). The ampoule was evacuated a third time to 10^{-6} torr and then backfilled with N_2. The last pump down was to 10^{-6} torr. It was then baked out a second time at 900°C for 10 minutes in the same position as before. In order to reduce water vapor and permit outgassing, the ampoule was pumped on overnight. The next day the ampoule was vacuum sealed. Then the Zn and Ga_2O_3 were mixed with the Ga and GaP by tipping the ampoule.

The crystals were grown in a temperature gradient to prevent homogeneous nucleation. Figure 6 shows the temperature profile in which the crystals were grown to be a 25°C gradient from the bottom of the ampoule to the top, so that the crystals would nucleate at the bottom. Experimental results have shown that this gradient reduces voids and liquid Ga inclusions in the GaP single crystals and produces large single crystals [30].

---

* The N_2 and H_2 were purchased from Matheson Scientific Inc.

For the crystal growth operation, the vacuum sealed ampoule was placed into the cold furnace. The furnace was then turned on and allowed to reach 1175°C at the bottom of the ampoule (1200°C at the top). It was held at 1175°C for 7 hours. Then the Trend Track* was programmed to cool at 5°C per hour down to 800°C and at 200°C per hour to room temperature. As was indicated before, the actual temperature was monitored by 5 thermocouples placed at 1 inch intervals up from the bottom of the ampoule.

In order to recover the single crystals the ampoule was broken open and the excess liquid Ga was poured off. The charge was placed in nitric acid and boiled slowly for 5 minutes. It was then rinsed thoroughly with deionized water. After rinsing, the charge was then boiled slowly in a 50-50 volume solution of HCl and deionized water for 4-8 hours in order to dissolve the Ga. Finally, the crystals were rinsed thoroughly in deionized water. A photograph of the ampoule, charge, and a recovered single crystal of GaP is shown in Figure 8.

Potentially good crystals were selected and lapped on one side with M302 (20 micron) Al_2O_3 abrasive** to develop a flat area, and then mounted on a lapping jig with glyclo-phthalate***, a low melting point wax. The second face was lapped successively with M302 (20 micron) and M305 (15 micron) Al_2O_3 abrasive to approximately

---

* Purchased from Leeds and Northrup

** Purchased from American Optical

*** Purchased from Aremco Products, Inc.

.015 inches thick. The samples were then polished with 3 micron and .1 micron diamond polishing compound respectively. The samples were cleaned with Alconox,* deionized water, and acetone.

The samples that were used for optical measurements were then cut with an ultrasonic grinder in the shape of a clover leaf. A photograph of the tool configuration and a clover leaf cut sample are shown in Figure 9.

After cleaning the samples thoroughly (see Appendix B) a film of SiO_2, 3500 Å thick, was R.F. vacuum sputtered on both sides of the sample in a Mathis SP 310 Sputtering Module. A few of the samples were anisotropically etched with aqua regia for 15 seconds and examined for pin holes but none were detected. The SiO_2 was sputtered on both sides of the sample to reduce out diffusion of components such as Zn, O_2 and P, and to reduce contamination [31]. As discussed in a latter section, the SiO_2 film should also strengthen the samples and reduce surface degradation.

The annealing was performed with the same equipment that was used for crystal growing. The furnace was, however, adjusted to have a 4 inch flat zone in the middle at 400°C, 600°C, or 900°C. The samples were loaded into a quartz test tube and connected to the vacuum station by a Cajon ultra-torr fitting and evacuated to 10^{-6}

---

* Purchased from Corco Chemical Company

torr. The system was then back filled to 1 atmosphere with ultra high purity argon* that was brought through valve A as shown in Figure 5. After closing the valves the samples were annealed at the desired temperatures and times.

Once the annealing cycle was completed, the test tube with the samples inside, was plunged into tap water for a rapid quench that would hopefully freeze in some non-equilibrium number of Zn-O complexes determined by the annealing cycle. The anneal time was defined as that time that the samples were within 2% of the anneal temperature as approximated by a thermocouple placed in the furnace adjacent to the system.

---

* Purchased from Matheson Scientific, Inc.

III RESISTIVITY AND HALL EFFECT, PHOTOLUMINESCENT SPECTRAL RESPONSE AND PHOTOLUMINESCENT EFFICIENCY

The resistivity and the Hall effect measurements were made on nominally rectangular plates of uniform thickness by the van der Pauw [32] technique. Visual examination indicated that the samples were homogeneous with few voids or inclusions. The contacts were placed at the edge of the sample opposite each other at the center of the sides of the rectangle. The actual contact was formed by discharging a 1μf capacitor through Be-Cu contacts to make a welded joint. The expression for resistivity is as follows:

$$\rho = \left(\frac{\pi d}{\ln 2}\right)\left\{\frac{V_{CD}/I_{AB}+V_{DA}/I_{BC}}{2}\right\} f\left(\frac{V_{CD}/I_{AB}}{V_{DA}/I_{BC}}\right) \qquad (6)$$

where f is a function of the ratio $\left[\frac{V_{CD}/I_{AB}}{V_{DA}/I_{BC}}\right]$ only and satisfies the relation

$$\left(\frac{V_{CD}/I_{AB}-V_{DA}/I_{BC}}{V_{CD}/I_{AB}+V_{DA}/I_{BC}}\right) = f \operatorname{arccosh}\left\{\frac{\exp(\ln 2/f)}{2}\right\} . \qquad (7)$$

ρ is the specific resistivity, d is the thickness, and V_{CD} and I_{AB} are voltages and currents as described in the original paper by van der Pauw [32].

A current of .5 ma was supplied by a constant current power supply, and was monitored by a Rawsen, model # 7632, dc ammeter (Figure 10). A Hewlett Packard, model 130C, scope was used to verify that good ohmic contacts had been made on the samples before the measurements were made. Since four contacts were necessary, all four voltage drops were measured in order that two resistivity measurements could be calculated for each sample for a consistency check. The voltages were read by a Dana, model 5400, digital voltmeter.

The Hall mobility was determined by measuring the change in voltage ΔV_{AC} when a magnetic field was applied perpendicular to the sample. Both the forward and reverse voltages were read to eliminate the inherent potential difference of the two points. The Hall mobility is given by

$$\mu_H = \frac{d}{B} \frac{\Delta V_{AC}}{\rho I_{BD}} \qquad (8)$$

where B is the magnetic induction and ΔV_{AC} is the change of voltage due to the magnetic field. A 5000 gauss magnetic field was obtained by a power supply designed by R. V. Gordman of BTL. The magnet had 3 inch diameter faces and had a 2 inch gap. The same constant current power supply was used to supply a current of .5 ma and the same ammeter was used for monitoring the current. The voltages were read with the Dana digital voltmeter Again, consistency checks were made on all the samples since four voltage changes were read.

The Hall coefficient, R, was calculated from the resistivity and the mobility.

$$R = \mu_H \rho \qquad (9)$$

Knowing the Hall coefficient, the carrier concentration was calculated.

$$n_e = 1/qR \qquad (10)$$

Once the data had been taken, it was used as input data for a Fortran program.

The excitation source for the photoluminescent spectra measurements was a Coherent Radiation, model 52, 2 watt argon laser. A photograph of the optical equipment is shown in Figure 11 and a

schematic of the photoluminescent spectra equipment is shown in Figure 12. The 4880 Å line was used for excitation of the sample and it has a beam diameter of 1.6 millimeter with a beam divergence of .5 milliradians. The output power was monitored by a Coherent Radiation, model 235, light sampler. The sampler split off 2% of the beam by passing the laser beam through a semi-reflective plate. The 2% of the light that was reflected from the front surface of the plate struck a Si solar panel that was monitored by a Dynascience, model 330, digital ammeter. The remaining part of the beam that was passed through the plate of the sampler was directed by mirrors, until it struck the sample which was located in a sample holder in the low temperature Janis dewar. The light path from the laser to the sample in the dewar is shown in the photograph. The measurements were made at liquid N_2 temperature in order to obtain better resolution. The sample holder had a hole slightly smaller than the center portion of the clover leaf.

The luminescent energy emitted by the sample passed through a filter in order to remove any laser light (all light below 5500 Å), and was then focused by the lens, onto the slit entrance of the monochromator The Spex 1800M, 3/4 meter Czerny Turner monochromator has a resolution capability of .09Å to .12Å at 632Å. When the slits widths were opened to 1000 microns during the experimentation, the resolution was 10Å. The Bausch and Lomb grating has 1200 lines/mm. The stepping motor for scanning was capable of stepping in .05Å increments, but the actual steps used during experimentation were 10Å.

An ITT FW 118 photomultiplier tube was used in conjunction with the photon counting equipment designed by H. Pruett of Western Electric Company, Engineering Research Center, to detect the intensity of luminescent light output of the sample. The useful range of the photomultiplier tube extends beyond the 6000Å -11,000Å range used in experimentation. In order to reduce dark current noise (thermionic emission from the cathode), the photomultiplier tube was cooled to $-20^{o}C$ by a photomultiplier tube cooling housing.

The photons emitted by the sample,when the sample was excited by the laser, struck the cathode of the photomultiplier tube which was biased at 2000 volts. The pulse that arrived at the last stage of the photomultiplier tube was amplified by a two stage preamplifier as shown in Figure 13. The first stage of the preamplifier acted as a "capacitance buffer" and eliminated the need of subsequent clipping to reduce RC decay time to an acceptable level. The second stage was a complementary follower with low input capacitance, low output impedance, and a gain in excess of .95.

A Hewlett Packard, model 5216A, electronic counter which permitted frequency-ratio measurements with "multiple periods averaged" was used as the control center of the preset count type photon counting system.

The monochromator was set at the initial wavelength, 6000Å, and the electronic counter was turned on to initiate a cycle. When the preset number of counts of 10,000 had been reached, the electronic counter sent a "print" command to the data acquisition test set which recorded the time on a magnetic tape. The data acquisition test set

has a Hewlett Packard 2547 A data coupler that is connected to a Kennedy magnetic tape recorder. Simultaneously a signal was sent to the preset counter which controlled the stepping motor that advanced the monochromator in 10Å steps. Hold off commands were sent to the counter when data was being recorded and when the monochromator was being advanced. Once the hold-off command had been removed, the next signal pulse initiated a new cycle. This process continued until the 6000Å - 11,000Å spectral range had been recorded.

The photon counting equipment that was used has several improvements over previous light detection systems. First, counting discrete photons gives a better signal to noise ratio than current detection systems. Appendix C explains the theory of photon counting as well as giving an example showing the improved signal to noise ratio for photon counting. Second, by counting a fixed number of pulses rather than using a fixed time, a tremendous saving of time is insured. Using fixed interval photon counting, the time interval, τ, is determined by the length of time required to acquire a given signal to noise ratio for the weakest signal that is expected. If the signal rate were increased one hundred times, the same length of time is still required for each measurement interval. If a fixed number of pulses are counted to give a certain signal to noise ratio, it would take considerably less time to count at a wavelength with high light intensity than it would to count at a wavelength of low light intensity. The signal to noise ratio can be calculated from the relation that is developed in Appendix C:

$$\frac{S}{N} = \frac{N^{1/2}}{1 + r_d/r_s} \tag{11}$$

The number of counts taken was 10,000 which gave a signal to noise ratio of 50 when the signal was of the same intensity as the noise. This was the worst case encountered in experimentation.

Since time cannot be measured directly with an electronic counter, the number of time units 10^{-5} seconds long in a given period, n_2, were counted for the length of time it took to count 10,000 signal pulses, n_1, from the photomultiplier tube. n_2 was recorded on a magnetic tape of the data acquistion test set. The data from the magnetic tape was used as input data for the Fortran program. The program calculated the intensity from the relation:

$$r_s = \frac{f_2 n_1}{n_2} - r_d = \frac{(10^5)(10^4)}{n_2} - r_d = \frac{10^9}{n_2} - r_d \tag{12}$$

where r_s is the signal rate, f_2 is the electronic counter time base which was equal to 10^5 Hz, n_1 is the number of signal counts made, and r_d is the dark count rate. After every spectral run, n_2 was recorded for the dark current by closing the exit slit of the monochromator. This number was manually inserted into the program and it was reduced by the computer to r_d by using the relation:

$$r_d = \frac{f_2 n_1}{n_2} \tag{13}$$

The program also corrected for the nonlinear spectral response of the monochromator and the photomultiplier tube. This calibration was performed by scanning the light ouput of a EPl-1357 Eppley standard lamp. After each data point had been calibrated and the intensity

calculated, the program normalized the data. The final part of the program punched a paper tape that was run through a Digital Equipment Corporation PDP-9 computer to obtain a graph of the recorded spectra on a Calcomp plotter. Before making spectral measurements the laser optics and the system optics were adjusted for maximum luminescence. The output power of the laser was then adjusted in order that the counter would be counting approximately 500,000 pulses/second (this included dark current pulses and pulses due to sample luminescence) at a wavelength of 6900Å, the peak intensity. If the number of pulses being counted in a short time interval is too large, the counter would not be able to discriminate between some of the pulses which would result in part of the pulses not being counted. On the other hand, if the number of pulses being counted in a short time interval is too small, it would take an unreasonable length of time to scan the spectrum. By using 500,000 counts/second, there were less than 2 per cent of the pulses not counted as determined by the relation

$$F = 1-e^{-t\alpha} \qquad (14)$$

where F is the fraction of pulses not counted, t is the rise time of the counter, (40 nanoseconds), and α is the number of pulses being counted, (500,000 pulses/second) [33].

The photoluminescent efficiency was measured with a photoluminescent test set shown in the photograph of Figure 11 (black box in foreground) and in Figure 14. the sample was placed on a transparent platform in the middle of a reflective cavity that was enclosed in a light-proof

black box. The laser beam entered the black box and was focused by a lens on a semi-reflective prism that split the beam into two parts. The first part of the beam struck a calibrated Si solar cell which was used to monitor the input power. The solar cell was calibrated with an Eppley thermopile, number 9296. The remainder of the laser beam struck the sample. The luminescent energy emitted by the sample was measured by a calibrated Si solar cell panel consisting of 30 individual solar cells. The solar cell panel was calibrated with a GaP light emitting diode having a luminescent efficiency of 1.06% which was supplied by J. Jayson of Bell Telephone Laboratories.

Once the solar cell monitor and solar cell panel had been calibrated, the external quantum efficiency, η, could be calculated from the equation:

$$\eta = \frac{\text{photons out}}{\text{photons in}} = \frac{A\ V_{scp}}{B\ V_{scm}} = 2.70\ \frac{V_{scp}}{V_{scm}} \qquad (15)$$

where A is the constant of calibration used to determine output power, V_{scp} is the voltage of the solar cell panel, B is the constant of calibration used to determine input power, and V_{scm} is the voltage of the solar cell monitor.

The constant A takes into effect the losses of the reflecting cavity and the solar cell panel calibration. The output power of a diode [34] can be written:

$$\Phi = \frac{\eta_D I_D hc}{\bar{\lambda} e} = 18.58\%\ \text{mw} \qquad (16)$$

where Φ = output power of the diode,

η_D = 1.06 %, calibrated diode efficiency,

I_D = 10ma, current into the diode,

h = 6.63 X 10^{-34} joule•second, Planck's constant,

c = 3 X 10^{8} m/second, speed of light,

$\bar{\lambda}$ = 7100 Å, average output wavelength of the diode,

e = 1.6 X 10^{-19} amp•second, charge of an electron.

Once Φ has been calculated, A can be determined from the following equation:

$$A = \frac{\Phi}{V'_{scp}} = 1.864\% \text{ mw/mv} \qquad (17)$$

where V'_{scp} (9.97 mv) was the voltage reading of the solar cell panel when the diode was placed in the sample position with 10 ma of current passing through it.

The constant B takes into effect the solar cell monitor calibration and can be written

$$B = \frac{V'_{scc}\ V_{TP}}{V_{scm}\ V'_{sc}\ S_{TP}} = .689\ \frac{mw}{mv} \qquad (18)$$

where V'_{scc} = 10.6 mv, the voltage of the standard solar cell in the sample position when illuminated with part of the laser beam split by the prism,

V_{TP} = .269 mv, the voltage of the Eppley thermopile when placed in front of the black box and illuminated with the laser,

V_{scm} = .580 mv, the voltage of the monitor in the black box when illuminated with part of the split light from the laser beam,

V'_{sc} = 15.08 mv, the voltage of the standard solar cell placed in front of black box when illuminated with the laser beam,

S_{TP} = .472 mv/mw, the sensitivity of the Eppley thermopile supplied by Eppley.

All the voltages were measured by a Hewlett Packard, model 419A,DC null voltmeter that was interconnected to a Fluke, model 8100A, digital multimeter to give an accurate digital readout. The solar cell leads were reversed and the two readings were averaged to eliminate residual voltages. Several measurements were made and the values were averaged.

Before any measurements were taken, the experimental samples were set to a "time equal zero condition" (t = 0) by annealing at 900°C for 10 minutes. Both photoluminescent efficiency and spectra measurements were made after every anneal cycle. One group of samples was annealed at 400°C in 30 minute increments up to t = 4 hours (total anneal time). The anneal cycle was then continued in four hour increments to 24 hours. A second set of samples was annealed in four hour increments to t = 12 hours at 600°C. A few uncoated samples were annealed in 15 minute increments to t = 1 hour and then in four hour increments to t = 12 hours. After measurements at t = 12 hours, the samples were etched in a solution of 1 part concentrated H_2SO_4, 1 part 3% H_2O_2 and 3 parts H_2O for three minutes and measured again to determine degradation. A final experiment was performed to determine if the initial (t = 0) condition could be reset. All of the photoluminescent efficiency and spectra measurements were made

by exciting the sample with the 4880 Å line of the laser. The efficiency measurements were made at room temperature but the spectra measurements were made at 77°K.

IV RESULTS AND DISCUSSION

Several samples of the raw materials purchased and the solution grown crystals were analyzed by optical emission spectroscopy employing a d-c arc technique with at least 20 mg of each sample being analyzed. Table I gives the analysis for each sample and Table II gives all of the impurities checked.

The raw materials were found to have more impurities than the analysis supplied with the material. The zinc was purchased from United Mineral and Chemical as being 99.9999% pure. Upon examination the zinc was found to have a heavy trace of copper and several trace impurities as shown in Table I.

It was found by emission spectroscopy that the gallium oxide purchased from Alusuisse as being 99.9999% pure had a heavy trace of phosphorus, a trace of silicon and magnesium, and a fine trace of several impurities as indicated in Table I.

The polycrystalline gallium phosphide that was purchased from Monsanto as being 99.9999% pure was found to have heavy traces of magnesium and aluminum, and fine traces of several impurities as indicated in Table I.

Emission spectroscopy did not show any impurities in the gallium purchased from Alusuisse as being 99.9999% pure.

The solution grown gallium phosphide single crystals had only barium and chromium as fine trace impurities that were not found in the raw material (Table I). All of the other impurities could be attributed to the raw materials. In fact, magnesium and aluminum were reduced

considerably by the growth process. These results were verified by examining more of the raw materials and solution grown crystals.

Emission spectroscopy did not reveal any detectable loss of zinc when one sample was annealed at 900°C for 30 minutes.

X-ray methods were used to identify both the composition and orientation of the grown crystals. Debye-Scherrer patterns revealed the samples to be gallium phosphide. Laue photographs confirmed that the samples were gallium phosphide single crystals with the faces being parallel to a (111) plane.

Resistivity and Hall effect measurements were made on five samples as shown in Table III. Each resistivity measurement in Table IV represents an average value of the four different measurements made on each sample. The precision of measurement of each sample was determined from the percentage difference in resistivity from the average resistivity calculated. As can be seen, sample #2 has the highest percentage difference, 0.22%. The resistivity of the five samples varied from 0.0854 ohm·cm to 0.228 ohm·cm with an average resistivity of 0.129 ohm·cm for all the samples. The average Hall coefficient was 8.61 cc/coulomb and the range was 4.7 cc/coulomb to 12.1 cc/coulomb. One of the samples showed Hall measurements have a percentage difference of 60%.* The average carrier concentration was 8.10×10^{17}/cc with a range from 5.17×10^{17}/cc to 13.3×10^{17}/cc. The mobility varied from 50.0 cm^2/volt·sec to 111.6 cm^2/volt·sec with an average mobility of

* Most of this variation can be explained by the small change in voltage due to the magnetic field as compared to the large potential difference of the sample, i.e., reading μv on a mv scale. This situation could be rectified by nulling the potential difference of the sample with a "bucking" voltage.

70.0 cm^2/volt·sec. This difference in carrier concentration and mobility probably accounts for the differences in quantum efficiency observed on the measured samples. The values of carrier concentration and mobility are consistent with the values of solution grown crystals published in the literature [35].

As can be seen from Figure 15, the external quantum efficiency of sample H-140, coated with a thin SiO_2 film increased rapidly with anneal time at a 400°C. A peak in total quantum efficiency was reached after an annealing time of one hour that was over three times greater than the as quenched (t=0) efficiency. In order to verify the phenomena, several other samples were analyzed and they exhibited this same short time, low annealing temperature efficiency peak (Table V). This efficiency peak will be discussed later. The efficiency decreased rapidly from one hour to two hours, reaching its lowest value after four hours of annealing. A second efficiency peak was reached after 16 hours of annealing, which was almost four times greater than the as quenched efficiency. There was a slight degradation in efficiency as time of anneal was increased beyond 16 hours. Based on the data for the other samples studied, the efficiency curve was smooth between 8 and 16 hours of annealing.

By referring to Figures 16 thru 18 which show the normalized intensity plotted as a function of wavelength for t=0, t=4 hours, and t=20 hours respectively, it can be seen that for sample H-140, annealed at 400°C, the emission of the infra-red intensity (9200Å) is decreasing with annealing time while the emission of the red peak (6900 Å) is

relatively unchanged. As was discussed earlier, the infra-red emission is the result of ionized oxygen donors recombining with ionized zinc acceptors, while the red emission at 77°K (liquid nitrogen temperature) is the result of exciton recombination. The area under the curve was measured for both the red emission and the infra-red emission and their ratios are recorded in Table VI. In Figure 19, the integrated intensity ratio is plotted as a function of annealing time at 400°C for sample H-140. There was a 36% increase in the intensity ratio for the first four hours of annealing. From four hours to twenty hours of annealing the red to infra-red intensity ratio increased by almost 8 times. Beyond twenty hours of annealing the intensity ratio increased by less than 10%.

A second set of samples were studied at an annealing temperature of 600°C. Quantum efficiency is presented in Table VII, and quantum efficiency versus annealing time for sample H-121 is plotted in Figure 20. After the first anneal cycle of four hours, the efficiency had reached its maximum value. Upon further annealing a very slight degradation was observed on some of the samples. There are two important differences between the 400°C anneal and the 600°C anneal (excluding the short time peak at 400°C). First, it took less than 4 hours to reach the peak efficiency at 600°C, while it took 16 hours to reach the peak efficiency at 400°C. Second, the efficiency increased by 3.8 times at 400°C, but it only increased 1.75 times at 600°C. It took longer to reach the peak efficiency, but the increase in efficiency was greater at 400°C than at 600°C.

The normalized emission intensity is plotted as a function of wavelength for sample H-121 annealed at 600°C for four hours (Figure 21). The integrated intensity ratio of the red to infra-red emission was measured for several samples and the data is presented in Table VIII. In Figure 22 the corresponding ratio is plotted versus annealing time for sample H-121. Within four hours the intensity ratio had reached 98% of its maximum value. It took less than four hours for the intensity ratio to reach an equilibrium value at 600°C while it took more than 20 hours for the equilibrium value to be reached at 400°C. Second, the intensity ratio increased 14 times at 400°C, but it increased only four times at 600°C. The 400°C annealing temperature had a larger intensity ratio than the 600°C annealing temperature, but the lower temperature took longer to reach an equilibrium concentration of complexes than the higher temperature. The relationship between the quantum efficiency and the intensity ratio will be discussed later.

The photoluminescent spectra measurements exhibited the same trend that Onton and Lorenz [24] reported for electroluminescent spectra measurements although there were some experimental differences. It should be remembered, however, that Onton and Lorenz studied diodes by electroluminescence rather than bulk material by photoluminescence. They made their measurements at 125°C after a 600°C anneal cycle without correcting for the spectra response of the spectrometer. Although they did not coat their samples with protective films of SiO_2, their samples were etched in aqua regia after every heat treatment to

minimize effects caused by surface conditions. Onton and Lorenz not only observed a change of electroluminescent emission from the infra-red peak to the red peak at 600°C, but they also reported an increase in electroluminescent efficiency. This increase in total efficiency is consistent with the experimental results obtained for photoluminescent efficiency in the present investigation.

As was mentioned earlier the emission peak at 6900Å (red) is attributed to exciton recombination, while the emission peak at 9200Å is attributed to an ionized oxygen donor recombining with an ionized zinc acceptor (infra-red).* The equilibrium number of Zn-O complexes that formed will depend on the annealing temperature. The calculation of the equilibrium number of Zn-O complexes formed in GaP for different temperatures using a discrete lattice approach has been developed by J. Wiley [36] from a method used by Lidiard [37] for the calculation of ion-vacancy complexes in NaCl.

In the simplest model, formation of Zn-O complexes is promoted by the coulomb attraction between the zinc and oxygen, but is opposed by the randomizing thermal process in the system. The Helmholtz Free Energy, F, is given by

$$F = E - TS = E - kT\ln W \qquad (18)$$

---

* Recently R.N. Bhargava, BTL, has indicated in an article to be published that the infra-red emission is the result of a bound electron at an oxygen site recombining with a free hole in the valence band. This would not change the results or the interpretation of the results if this were the true infra-red recombination mechanism.

where W is the number of distinguishable ways of constructing the system, and E is the total energy of the system which, for the time being, will be taken to be solely the coulomb interaction energy of the Zn-O complexes. The total energy, E, is defined as

$$E = \frac{P_1 e^2}{\epsilon a_1} \tag{19}$$

where P_1 is the concentration of Zn-O complexes ("first neighbor pairs"), e is the electronic charge, ϵ is the dielectric constant, and a_1, is the Zn-O separation distance. The entropy term, W, is given by

$$W = \left[\frac{Z_1^{P_1} \prod_{S=0}^{P_1-1} (N-S)}{P_1!}\right]\left[\frac{(N-P_1)!}{(N-N_A)!(N_A-P_1)!}\right]\left[\frac{(N-P_1)!}{(N-N_D)!(N_D-P_1)!}\right] \tag{20}$$

The first bracketed term is the number of distinct ways of arranging P_1 pairs in the lattice by putting one member of the pair on one of the N sites of one sublattice and the other member of the pair on one of the Z_1 nearest-neighbor sites of the opposite sublattice (for GaP $Z_1 = 4$). Having placed the P_1 pairs, there are now $[N - N_A]$ Ga atoms and $N_A - P_1$ acceptors to be placed on the $N - P_1$ vacant Ga sites. The number of distinct ways of filling these Ga sites is given in the second bracketed term. The third term applies to the $N - P_1$ remaining P sites in analogy to the Ga sites. By substituting Eqs. (19) and (20) into Eq. (18) and by minimizing F by setting $dF/dP_1 = 0$, the equilibrium concentration of Zn-O pairs, P_1, is

$$\frac{P_1}{(N_A-P_1)(N_D-P_1)} \simeq \frac{Z_1}{N} \exp \frac{e^2}{\epsilon a_1 kT} \tag{21}$$

Stirling's approximation and the approximation $P_1 \ll N$ (an excellent

approximation since $N \simeq 2.5 \times 10^{22}$ sites/cm^3 and P_1 is of the order of the doping level which is typically 10^{18} atoms/cm^3) was used.

Until now only first neighbor pairs, P_1 and coulombic interactions between paired ions have been considered. Two generalizations are easy at this point. The "unpaired" ions interact with each other and this energy should be included in E. The easiest way to handle this is to calculate explicitly the fraction of ions paired as first, second, third,..., n^{th} neighbors and then allow the remaining ions to interact with each other in a collective or Debye-Hückel atmosphere (the + ions tend to cluster around the - ions and vice-versa thus lowering the total energy) [37-38].

Eq. (20) can be rewritten for the explicit calculation of pairs out to l^{th} neighbors as follows:

$$W = \prod_{j=1}^{l} \frac{Z_j^{P_j} \prod_{S=0}^{P_j-1} (N-S-\beta)}{P_j!} \frac{[(N-\beta)!]^2}{(N_A-\beta)!(N_D-\beta)!(N-N_A)!(N-N_D)!} \tag{22}$$

where

$$\beta \equiv \sum_{k=1} P_k \tag{23}$$

The total energy of the system can be written in the form

$$E = -\sum_{j}^{l} \frac{P_j e^2}{a_j} + E_{DH} \tag{24}$$

where E_{DH} is the Debye-Hückel term that depends on the number of ions paired and hence must be included in an iterative or self-consistent way. The Debye-Hückel energy term is developed in reference [37]. It is easy to include the free holes in E_{DH} (they are charged and hence

interact with the charged donors and acceptors) and to include the effects of screening by holes and unassociated ions. This latter effect is small at typical doping levels and has not been included in the calculations performed so far.

By making use of Stirling's approximation and $P_1 \ll N$ as done before it can be shown that, for $j = 1,2,\ldots l$,

$$\frac{P_j}{(N_A-\beta)(N_D-\beta)} = \frac{Z_j}{N} \exp \alpha_j = \Omega_j \tag{25}$$

where

$$\alpha_j = \frac{e^2}{\epsilon a_j kT} \tag{26}$$

The Debye-Hückel term serves only to alter a_j (lowering it slightly). In practice only five shells of neighbors in the explicit pairing (i.e., $l=5$), need to be considered. Any ions separated by more than that amount a_j are included in the Debye-Hückel "atmosphere". In order to calculate P_1 observe that

$$\frac{P_j}{P_1} = \frac{\Omega_j}{\Omega_1} = \frac{Z_j}{Z_1} \exp (\alpha_j-\alpha_1) \tag{27}$$

These ratios are directly calculable (iterative techniques are required) and allow β to be written as

$$\beta = P_1 \sum_{k=1}^{l} \frac{\Omega_j}{\Omega_1} = P_1 S \tag{28}$$

Thus

$$\frac{P_1}{(N_A-P_1S)(N_D-P_1S)} = \frac{Z_1}{N} \exp \alpha_1 \tag{29}$$

and higher order pairs are easily calculated from Eq. (27). From the calculations at 900°C the ratio P_2/P_1 is less than .1, P_3P_1 is less than .05, etc. which indicates that nearly all pairs are nearest neighbor pairs. At high temperatures P_1 <u>itself</u> is small and so is the <u>total</u> pairing. The theoretical curve for GaP in Figure 23 was calculated using Eqs. (22) to (29) and calculating pairs explicitly through 5th neighbors. The relevant lattice parameters and neighboring sites for GaP are listed in Table IX.

Wiley plotted [pairs]/[O] ratio versus temperature for nominal doping concentrations of 6 X 10^{16}/cc of oxygen and 1 X 10^{18}/cc of zinc [39]. The carrier concentration for the present studies was measured to be 8.12 X 10^{17}/cc. The axis was relabeled as I_R/I_{I-R} since the red emission is attributed to Zn-O pairs and the infra-red emission is attributed to ionized oxygen donors to ionized zinc acceptors.

The integrated intensity ratio for red emission to infra-red emission after the equilibrium number of pairs had been formed at 400°C, 600°C, and 900°C were superimposed on the theoretical curve. The experimental points were normalized* from the 400°C point. As can be seen from Figure 23, the experimental results are consistent with the theoretical curve, and thus further support the paired defect model.

---

* The normalization was done by reading the theoretical I_R/I_{I-R} ratio from Figure 23 for 400°C. A normalization factor was calculated by dividing Wiley's calculated pair ratio by the measured I_R/I_{I-R} at 400°C. The normalization factor was then multiplied by the measured I_R/I_{I-R} ratios at 600°C and 900°C and the respective numbers were plotted.

It also supports the assumption that only short range effects need to be considered and that the simplifying approximations that were made in the development of the theoretical equations are reasonable.

By normalizing the experimental points to a point on the theoretical curve, the experimental curve could be the same shape as the theoretical curve and could fit quite well even though in actuality the experimental curve might be shifted to a higher or lower ratio or to higher or lower temperature. Furthermore the red/infra-red emission ratio may depend not only on the Zn-O to O concentration ratio, but also on a number of other factors such as lifetime, etc. For these reasons the quantitative agreement obtained by normalizing the experimental data may be partially fortuitous.

A final experiment was performed to determine if the "t = 0 condition" could be reset. Sample H-140 was annealed at 900°C for 30 minutes, then quenched, in an attempt to reset the initial conditions. Intensity versus wavelength is plotted in Figure 24. On comparing Figure 24 with Figure 16, it can be seen that the reset and the original "t = 0 condition" are essentially the same. The original integrated red/infra-red intensity ratio at the "t = 0 condition" is 2.2 and the reset integrated intensity ratio is 2.4 At the present time it is impossible to tell whether the difference is a real difference or due to experimental error. The total external quantum efficiency at the initial "t = 0 condition" was 0.47% while the efficiency of the reset "t = 0 condition" was 0.81%.

If it were assumed that the only change that was occuring in annealing was the creation of Zn-O complexes from the ionized oxygen and zinc, it would be expected that the total efficiency would not change with annealing. There are at leaast three models that can account for the fact that the total efficiency did increase with annealing time. First, because fewer non-radiative transitions occur when competing with an exciton recombination than when competing with an ionized donor-to-acceptor recombination, the probability of an exciton recombination is greater than an ionized donor-to-acceptor recombination [1,21]. As more complexes are formed, the total efficiency would increase. Second, there may be interstitial oxygen in the crystal that, upon annealing, have enough energy to become substitutional oxygen impurities [40]. This would not affect the I_R/I_{I-R} ratio but would increase the total efficiency. Third, it is possible that some oxygen compounds exist in the crystal which are disassociated during annealing to form substitutional oxygen impurities.

It is possible to eliminate the third model because it is believed that there would not be sufficient thermal energy available to break up oxygen compounds. A complicating factor is the fact that the spectra measurements must be made at $77^{o}K$ to clearly resolve the red and infra-red emission bands, but the efficiency measurements could only be made at room temperature with existing apparatus. Since results from radiative lifetime and decay time experiments for sulfur and silicon [1,21] support the model that the probability for exciton recombination is greater than ionized donor-to-ionized acceptor

recombination, it is reasonable to propose this model to explain the increased efficiency with annealing time.

At an annealing temperature of 400°C more complexes are formed and, according to the model, should result in a larger percentage increase in total efficiency than is produced at 600°C. Experimental evidence supports this model. The probability model does not explain why the "t = 0 condition" could be approximately reset for the emission ratio measurements but could not be reset for total efficiency measurements.

Annealing at higher temperature results in creation of a higher density of vacancies. With such a higher vacancy density, it would be more probable for the interstitial oxygen atom to diffuse to a vacant lattice site to become a substitution impurity. Since the per cent increase in efficiency was smaller at 600°C than at 400°C, this model does not explain the experimental results. However, it could explain why the "t = 0 condition" could be reset for the emission ratio measurements but could not be reset for efficiency measurements. When the "t = 0 condition" was reset the newly created substitutional impurities would not be forced to become interstitial impurities. By utilizing both models, a better explanation of the results could be given.

It was mentioned earlier that a peak in total quantum efficiency was observed after one hour of annealing at 400°C for several samples. From the data and the figures, it can be seen that this peak is not related to Zn-O complexes. To further investigate this short term peak several samples were prepared that did not have a SiO_2 thin film (Table X and Table XI). For these uncoated samples the total

efficiency decreased during the first hour of annealing at 400°C. After four hours of annealing, the efficiency was still below the initial value. Sixteen hours of annealing were required before the efficiency reached the initial value. Upon etching one sample, the efficiency increased 18%. Integrated intensity ratio measurements inferred that the number of Zn-O complexes increased with annealing time; however, the equilibrium number of complexes increased by only a factor of five compared to a factor of 14 for the coated samples. This result suggests that effects such as compound formation or thermal surface degradation reduce the amount of light that can escape from the sample. Presumably, etching removes the old surface or degrated surface and increases the measured efficiency. Emission spectroscopy did not show a loss of zinc, but it was not possible to check for loss of oxygen. Loss of oxygen would result in the formation of fewer complexes, but it is unlikely that oxygen would be lost when zinc is evidently not lost. The one hour annealing peak at 400°C is somehow caused by the thin SiO_2 film, but no detailed explanation can be given at the present. It should be noted, however, that SiO_2 coated samples gave more reproducible results than uncoated samples and, therefore, coating is considered to be a successful method of minimizing the surface-condition problem.

V CONCLUSIONS

From the investigation of photoluminescent spectral response, it was found that at lower temperatures the red/infra-red emission ratio is larger than at higher annealing temperatures. In addition, the maximum intensity ratio was reached sooner at high temperatures than at low temperatures. The experimental results when compared with the theoretical calculations of Wiley [36] show the applicability of a paired-defect model and the appropriateness of nearest neighbor approximations. The experimental results are also in agreement with electroluminescent studies made on diodes by Onton and Lorenz [24]. This supports the model that red emission from exciton Zn-O complexes is enhanced at the expense of infra-red emission.

Other models were proposed to explain the remainder of the experimental results. First, it was proposed that the exciton Zn-O complex recombination is more probable than the ionized donor to ionized acceptor recombination. Thus, by annealing at lower temperatures and creating more complexes, the per cent increase in total quantum efficiency would be greater. The quantum efficiency increases at a slower rate at lower annealing temperatures. Again this is consistent with Zn-O complex formation because such formation is slower at a lower temperature as a consequence of the temperature-dependent diffusion rate of the mobile species that enters the complex. Second, it was proposed that some interstitial oxygen will diffuse to vacant substitution sites and increase the total efficiency. It is more

difficult for the substitutional oxygen to diffuse into interstitial sites. This accounts for why the total quantum efficiency cannot be reset to its original "t = 0 condition". Although the integrated intensity ratio of red to infra-red emission can be reset.

Finally, it was shown that coating with SiO_2 thin films provides a means for obtaining reproducable luminescence with heat treatment. It reduces surface degradation that results in lower total efficiency and eliminates the need of etching after every anneal cycle. In addition, it does have some effect that increases the efficiency significantly at short times when annealed at 400°C.

TABLE 1 EMISSION SPECTROSCOPY ANALYSIS

MATERIAL	PC	HT	T	FT
Zn	Zn	Cu		Si,Mg,Pb
Ga_2O_3	Ga	P	Si,Mg	Fe,Mn,Cu, Ca,Al
GaP (polycrystalline)	Ga	Mg,Al		Si,Fe,Cu, Ca
Ga	Ga			
GaP (solution grown single crystal)	Ga,P		Mg	Ba,Si,Al, Zn,Cr,Ca

PC = principal constituent

HT = heavy trace, 50 ppm-100 ppm

T = trace, 10 ppm-50 ppm

FT = fine trace, less than 10 ppm

TABLE II ELEMENTS EXAMINED BY EMISSION SPECTROSCOPY

Zn	Cu	Si	Mg	Pb
Sn	Ga	P	Fe	Mn
Ca	Al	Ba	Cr	Be
As	Pt	Co	In	W
V	Ag	Ni	B	Mo
Na	Cd	Bi	Sb	Ge
Zr				

TABLE III INPUT DATA FOR RESISTIVITY AND HALL MEASUREMENTS

SAMPLE	d (cm)	RESISTIVITY MEASUREMENTS (VOLTS) V_{CD}	V_{DA}	V_{AB}	V_{BC}	HALL MEASUREMENTS (VOLTS) V_{DB}	V_{BD}	V_{AC}	V_{CA}
1	.0672	.0004	.0035	.0035	.0004	.00313	.00309	.00310	.00315
2	.0626	.0035	.00110	.00109	.0035	.00240	.00248	.00248	.00243
3	.0670	.0059	.0022	.0022	.0059	.00362	.00370	.00379	.00370
4	.0672	.0067	.0002	.00019	.0067	.00647	.00653	.00653	.00649
5	.0672	.0042	.00057	.00056	.0042	.00360	.00369	.00369	.00360

TABLE IV RESISTIVITY, HALL COEFFICIENT, CARRIER CONCENTRATION, AND MOBILITY

SAMPLE	ρ_{ave} (OHM·CM)	DEVIATION FROM MEAN VALUE ρ (%)	R_H (CC/COULOMB)	DEVIATION FROM MEAN VALUE R_H (%)	n_e X10^{-17}(/CC)	μ_H (CM^2/VOLT·SEC)
1	.0854	0	4.7	33.3	13.3	55.1
2	.117	.22	8.14	60.0	7.68	69.8
3	.228	0	11.4	12.5	5.49	50.0
4	.106	.15	6.72	50.0	9.30	63.3
5	.108	.21	12.1	0	5.17	111.6
AVERAGE FOR 5 SAMPLES	.129		8.61		8.20	70.0

TABLE V ANNEAL TIME AND EFFICIENCY DATA FOR GaP SAMPLES COATED WITH SiO_2 ANNEALED AT 400°C

ANNEAL TIME MIN (HR)	EFFICIENCY PER CENT SAMPLE (H-140)	SAMPLE (H-143)	SAMPLE (H-144)	SAMPLE (H-145)	SAMPLE (H-146)	SAMPLE (H-147)
0	.47	.75	.74	1.16	.31	.77
30	1.19	1.59	1.30	1.67	1.09	1.81
60 (1)	1.53	1.52	1.16	1.34	.86	1.75
90	1.41	1.55	1.22	1.34	.72	1.63
120 (2)	1.27	1.46	1.21	1.30	.63	1.63
150	1.27					
180 (3)	1.27					
210	1.22					
240 (4)	1.24	1.34	.90			
480 (8)	1.34	1.48	.86			
720 (12)		1.58	.85			
960 (16)	1.81	1.63	1.09			
1200 (20)	1.76					
1440 (24)	1.78					
1680 (28)	1.73					
0 (RESET)	.81					

TABLE VI ANNEAL TIME AND SPECTRAL INTENSITY DATA FOR GaP SAMPLES COATED WITH SiO_2 ANNEALED AT 400° C

ANNEAL TIME MIN	RED TO INFRA-RED INTEGRATED INTENSITY RATIO					
	H-140	H-143	H-144	H-145	H-146	H-147
0	2.20	2.34	2.34	2.22	2.28	2.30
30		2.50	2.02	2.12	2.36	2.38
60		2.40	1.98	2.44	2.38	2.38
90						3.90
120	2.23					
150	2.44					
180	2.70					
210	2.90					
240	4.57	5.3	3.54			
480	7.46	11.8	7.08			
720		19.8				
960	23.6	25.6	19.2			
1200	26.8					
1440	29.4					
1680	29.1					
0 (RESET)	2.40					

TABLE VII ANNEAL TIME AND EFFICIENCY DATA FOR SiO_2 COATED GaP SAMPLES ANNEALED AT 600°C

ANNEAL TIME MIN	EFFICIENCY PER CENT (H-121)	(H-122)	(H-123)
0	(.92)	(.65)	(.68)
240	(1.60)	(1.71)	(1.85)
480	(1.60)	(1.63)	(1.75)
720	(1.60)	(1.57)	(1.60)

TABLE VIII ANNEAL TIME AND SPECTRAL INTENSITY DATA FOR SAMPLES COATED WITH SiO_2 ANNEALED AT 600°C

ANNEAL TIME	RED TO INFRA-RED INTEGRATED INTENSITY RATIO		
MIN	H-121	H-122	H-123
0	1.92	1.88	2.03
240	7.75	8.72	8.42
480	7.82	8.96	8.52
720	7.88	9.10	8.79

TABLE IX LATTICE PARAMETERS FOR GaP

j	a_j(Å)	Z_j
1	2.16	4
2	4.51	12
3	5.93	12
4	7.08	16
5	8.06	24

For j = 1, 2.16Å is approximated to be between 2.36Å and 1.97 Å (2.36Å is the nearest neighbor separation in GaP with no distortion and 1.97Å is the separation for severe distortion), and all other a_j values are based on a 5.45Å lattice constant.

TABLE X ANNEAL TIME AND EFFICIENCY DATA FOR UNCOATED GaP SAMPLES ANNEALED AT 400°C

ANNEAL TIME MIN		EFFICIENCY PER CENT (H-132)	(H-133)	(H-165)	(H-203)
0		1.42	1.57	1.0	.84
15		1.21	1.58	.84	.77
30		1.18	1.50	.71	.51
45		1.22	1.62	.68	.47
60		1.27	1.54	.49	.41
240		1.03	1.13		
960		1.49	1.37		
960	(after etch)	1.77			

TABLE XI ANNEAL TIME AND SPECTRAL INTENSITY DATA
FOR UNCOATED SAMPLES ANNEALED AT 400°C

ANNEAL TIME MIN	RED TO INFRA-RED INTEGRATED INTENSITY RATIO H-121
0	
60	3.33
240	9.25
960	15.0
960 (after etch)	15.2

FIGURE 1

VARIOUS RECOMBINATION MECHANISM: (A) BAND TO BAND (B) DONOR TO VALENCE BAND (C) CONDUCTOR BAND TO ACCEPTOR (D) DONOR TO ACCEPTOR

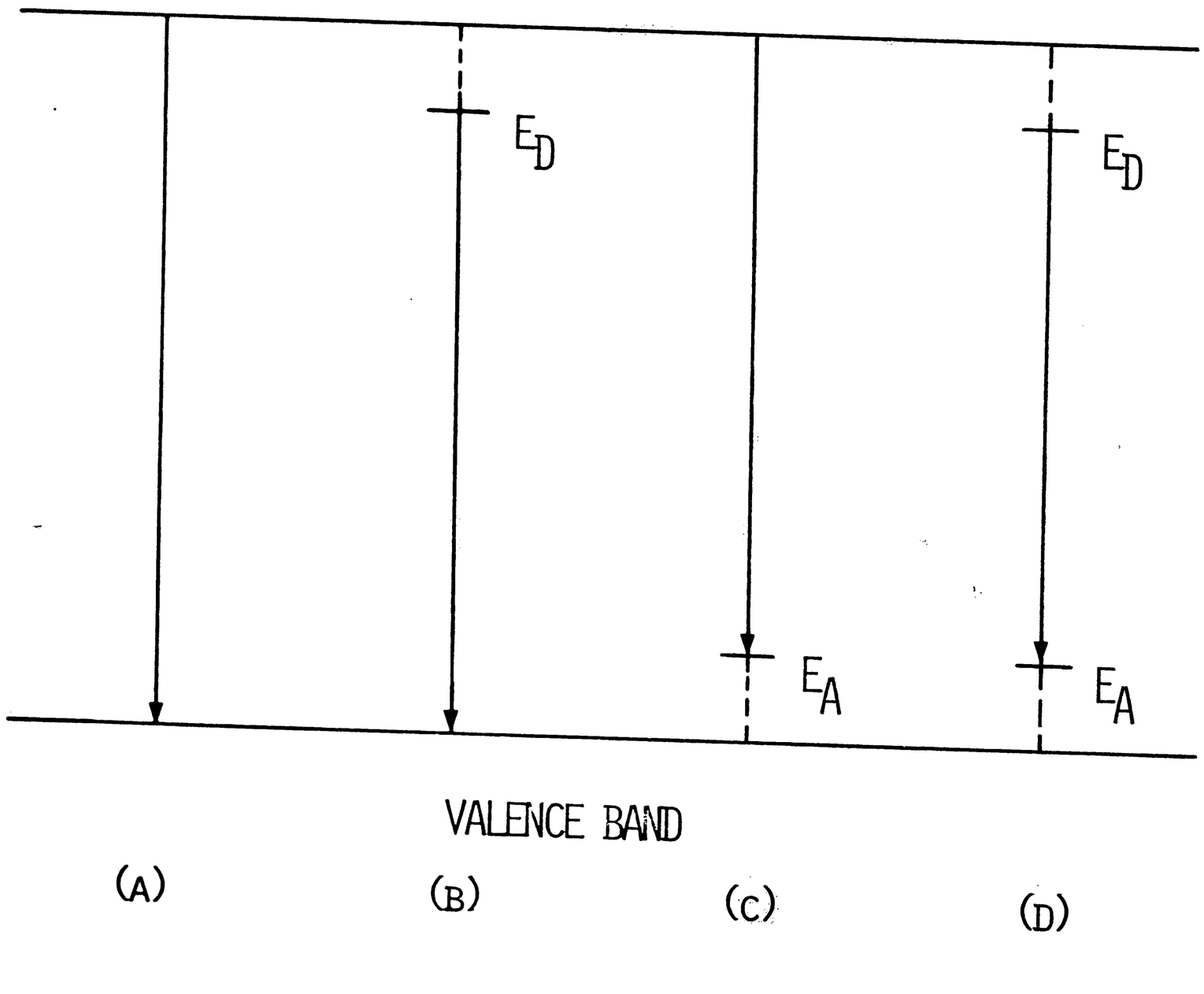

VARIOUS RECOMBINATION MECHANISM: (A) BAND TO BAND (B) DONOR TO VALENCE BAND (c) CONDUCTOR BAND TO ACCEPTOR (D) DONOR TO ACCEPTOR

FIGURE 2

ENERGY VS. MOMENTUM FOR (A) GaAs, DIRECT TRANSITION AND (B)

GaP, INDIRECT TRANSITION

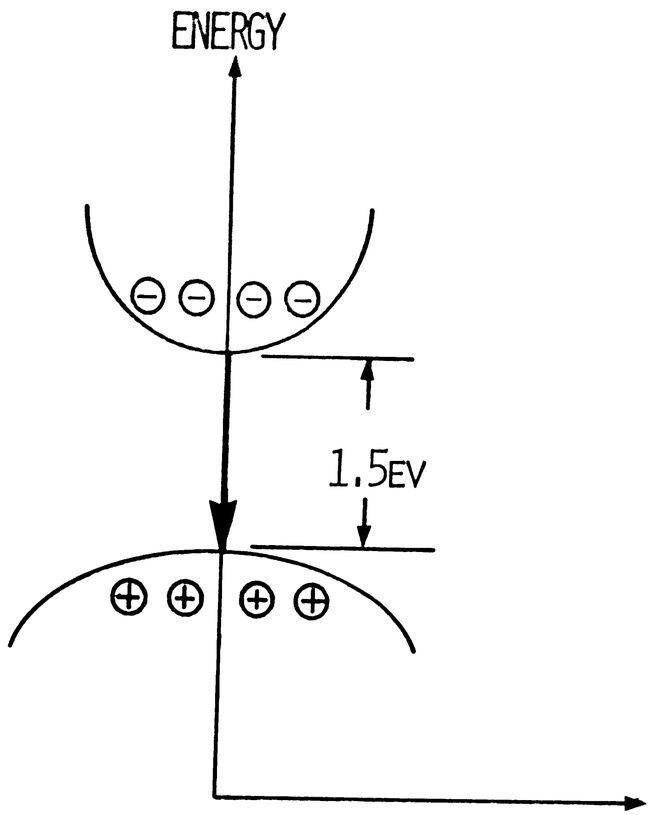

(A) GaAs

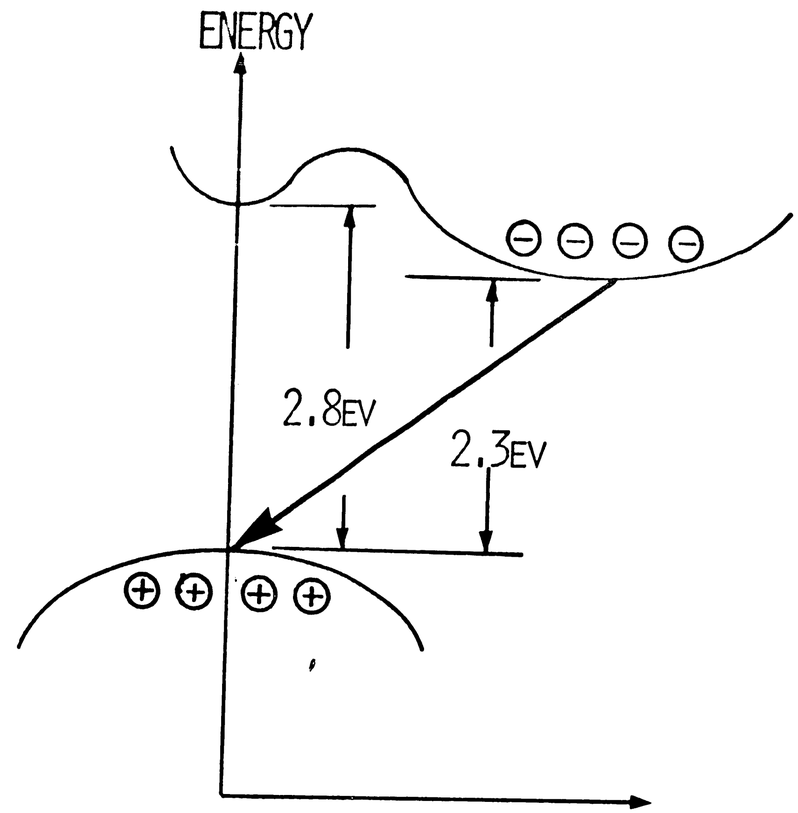

(B) GaP

ENERGY VS. MOMENTUM FOR (A) GaAs, DIRECT TRANSITION AND (B) GaP, INDIRECT TRANSITION

FIGURE 3

RADIATIVE RECOMBINATION MECHANISM IN ZN-DOPED GAP:

(A) DONOR-ACCEPTOR PAIR RECOMBINATION (INFRA-RED);

(B) EXCITON BOUND TO NEAREST NEIGHBOR ZN-O COMPLEX RECOMBINATION (RED);

(C) ELECTRON BOUND TO NEUTRAL ZN-O COMPLEX WITH HOLE TRAPPED AT DISTANT ZN ACCEPTOR PAIR RECOMBINATION (RED).

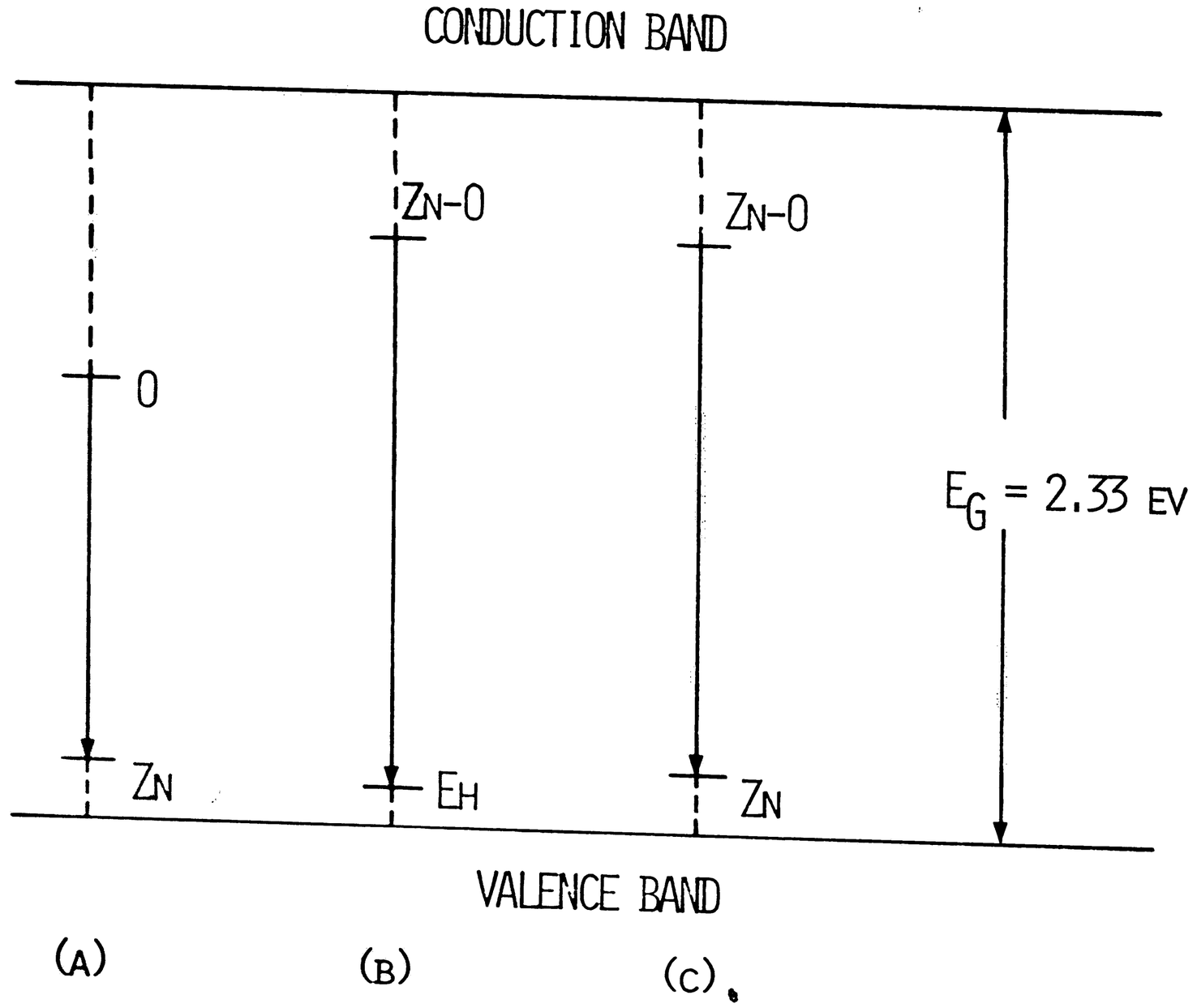

RADIATIVE RECOMBINATION MECHANISM IN ZN-DOPED GAP:

(A) DONOR-ACCEPTOR PAIR RECOMBINATION (INFRA-RED);

(B) EXCITON BOUND TO NEAREST NEIGHBOR ZN-O COMPLEX RECOMBINATION (RED);

(C) ELECTRON BOUND TO NEUTRAL ZN-O COMPLEX WITH HOLE TRAPPED AT DISTANT ZN ACCEPTOR PAIR RECOMBINATION (RED).

FIGURE 4

(A) THE EYE VISIBILITY GIVEN AS RELATIVE LUMINOISITY VS. WAVELENGTH.

(B) THE ELECTROLUMINESCENCE EMISSION AT 300°K FOR GaP (RED AND GREEN LIGHT).

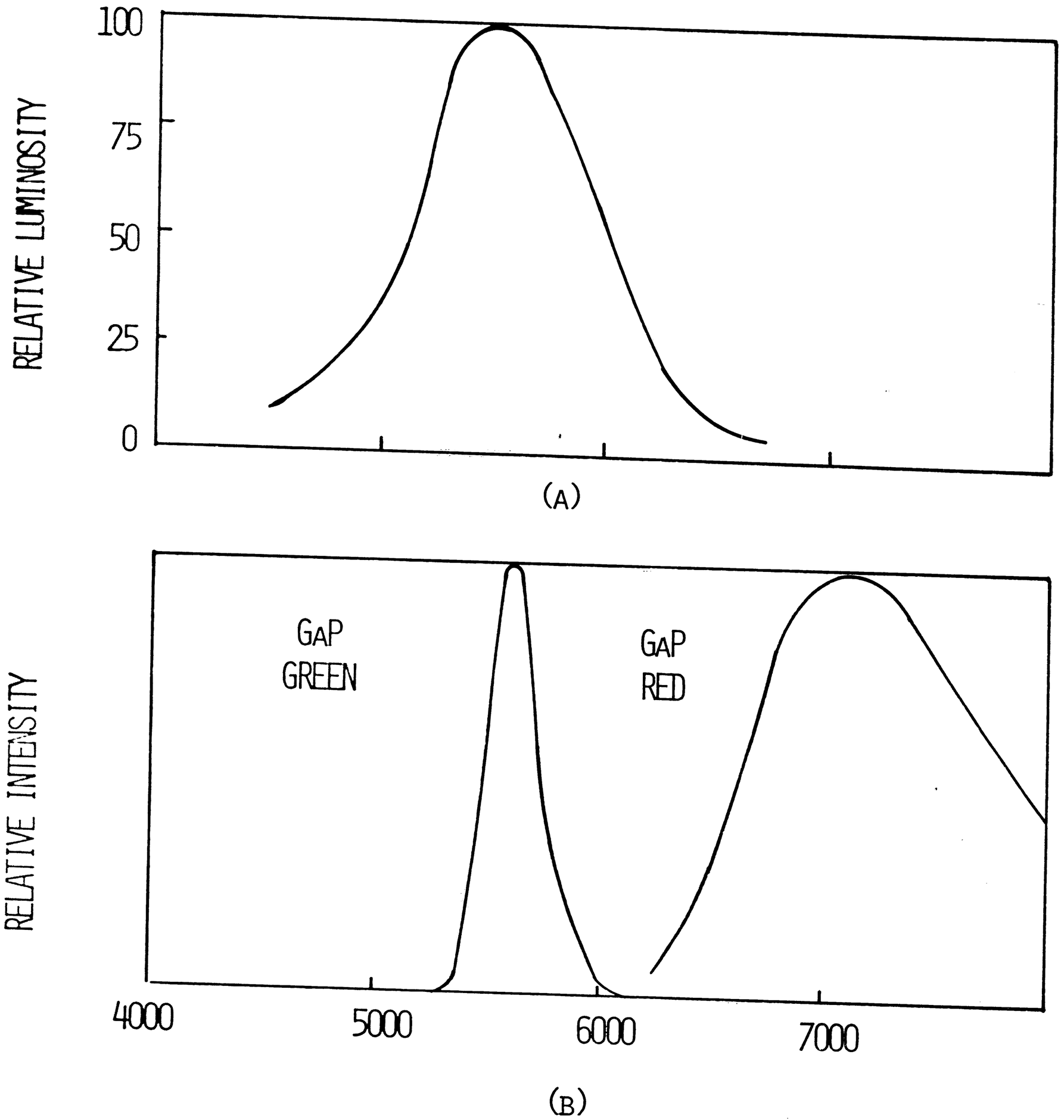

(A) THE EYE VISIBILITY GIVEN AS RELATIVE LUMINOISITY VS. WAVELENGTH.

(B) THE ELECTROLUMINESCENCE EMISSION AT 300°K FOR GaP (RED AND GREEN LIGHT).

FIGURE 5

CRYSTAL GROWING & ANNEALING APPARATUS

CRYSTAL GROWING & ANNEALING APPARATUS

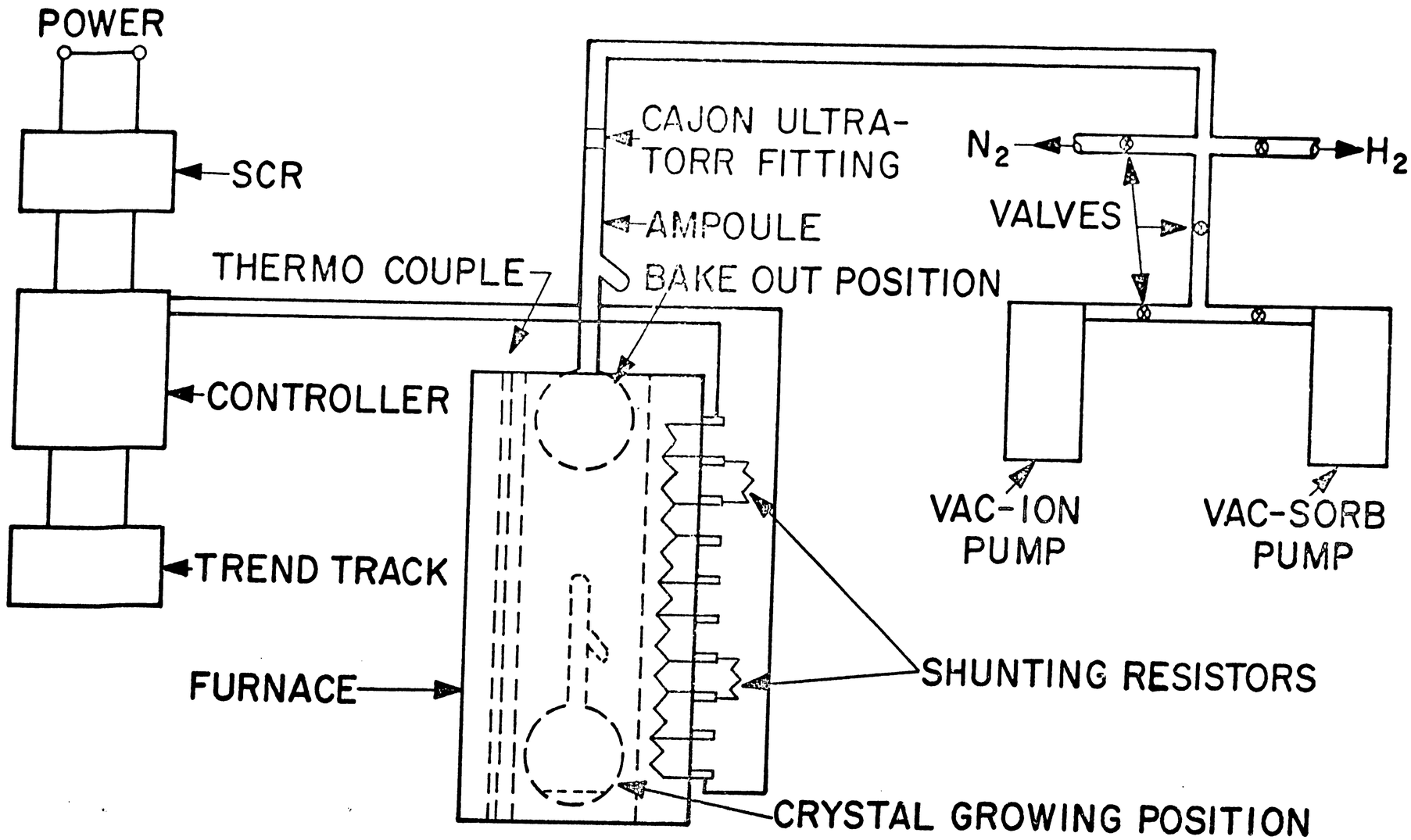

FIGURE 6

TEMPERATURE PROFILE FOR SOLUTION GROWN CRYSTALS

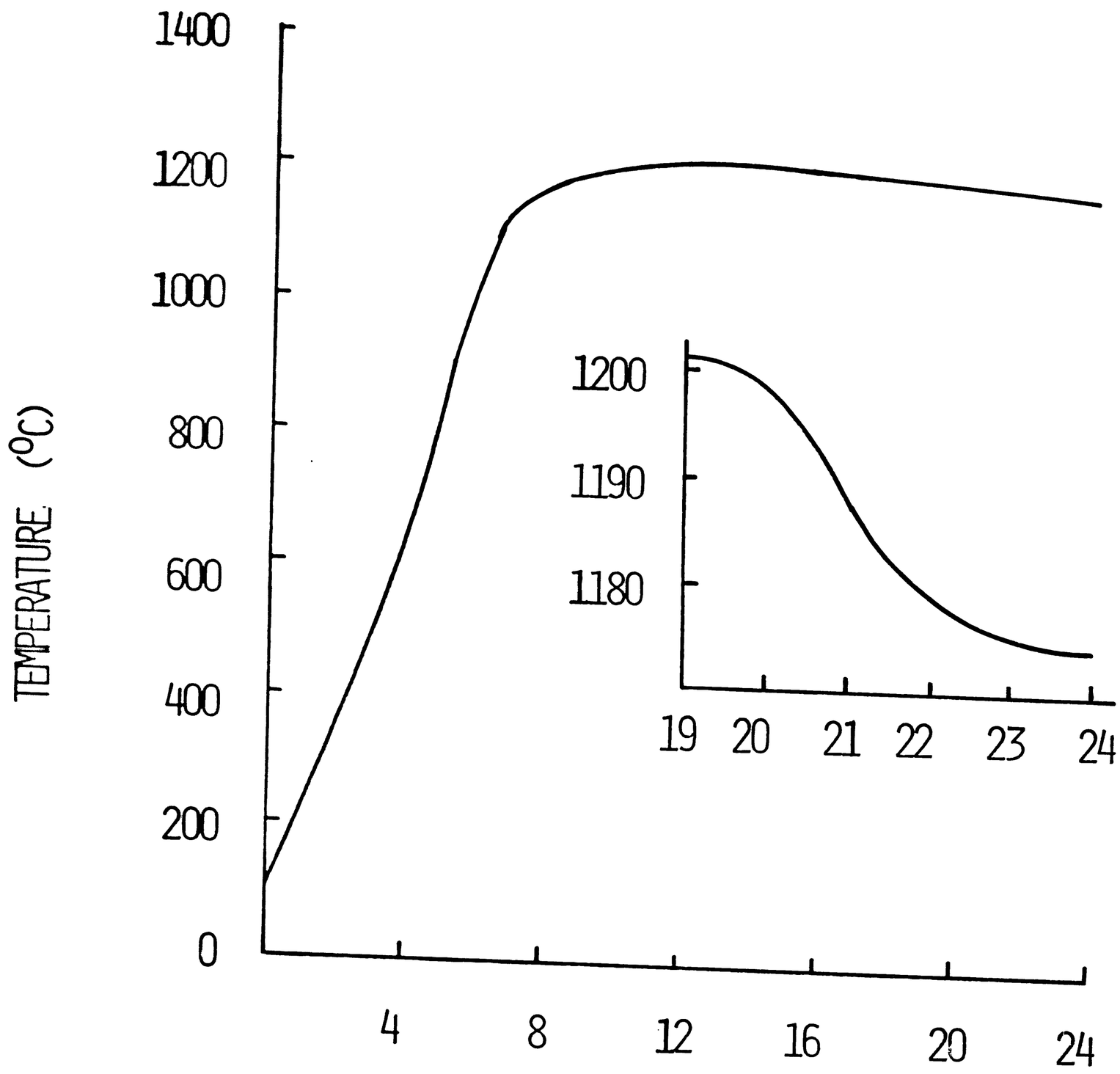

DISTANCE INTO FURNACE (INCHES)

TEMPERATURE PROFILE FOR SOLUTION GROWN CRYSTALS

FIGURE 7

TEMPERATURE VS. TIME PLOT FOR SOLUTION GROWN CRYSTALS

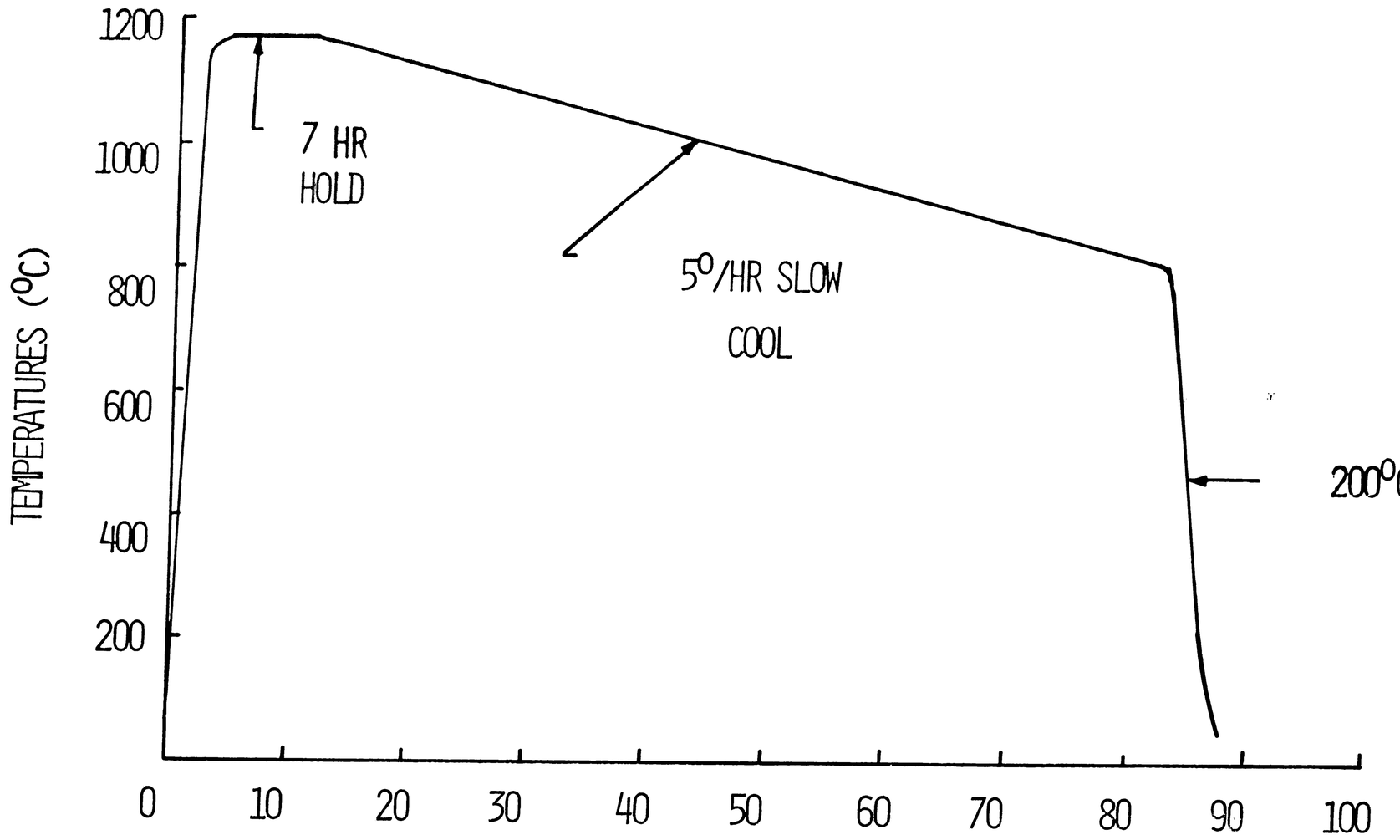

TEMPERATURE VS. TIME PLOT FOR SOLUTION GROWN CRYSTALS

FIGURE 8

CRYSTAL GROWING AMPOULE WITH RAW MATERIAL AND POLISHED SINGLE CRYSTALS

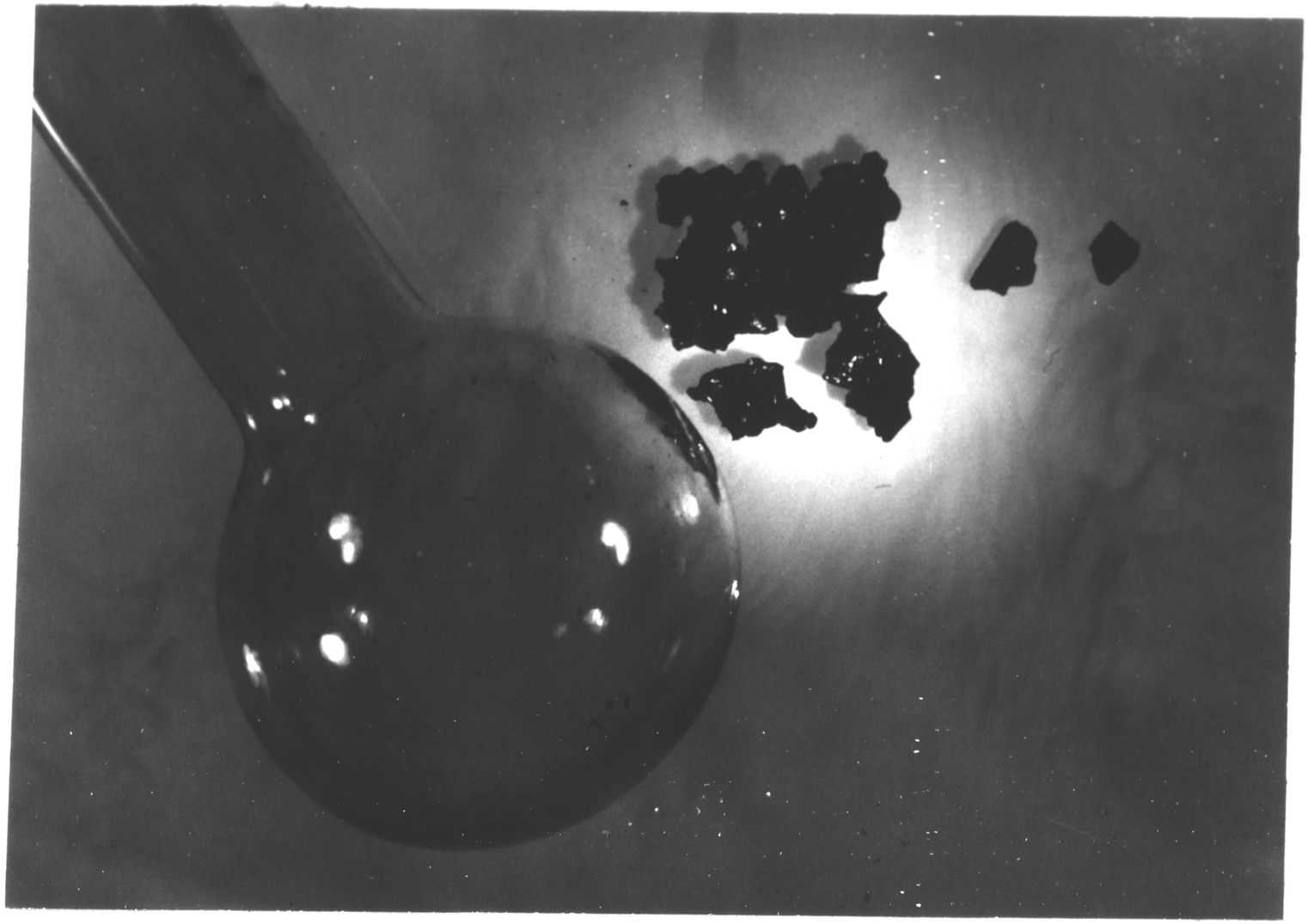

CRYSTAL GROWING AMPOULE WITH RAW MATERIAL AND POLISHED SINGLE CRYSTALS

FIGURE 9

CLOVER LEAF TOOL AND CLOVER LEAF CUT SAMPLE

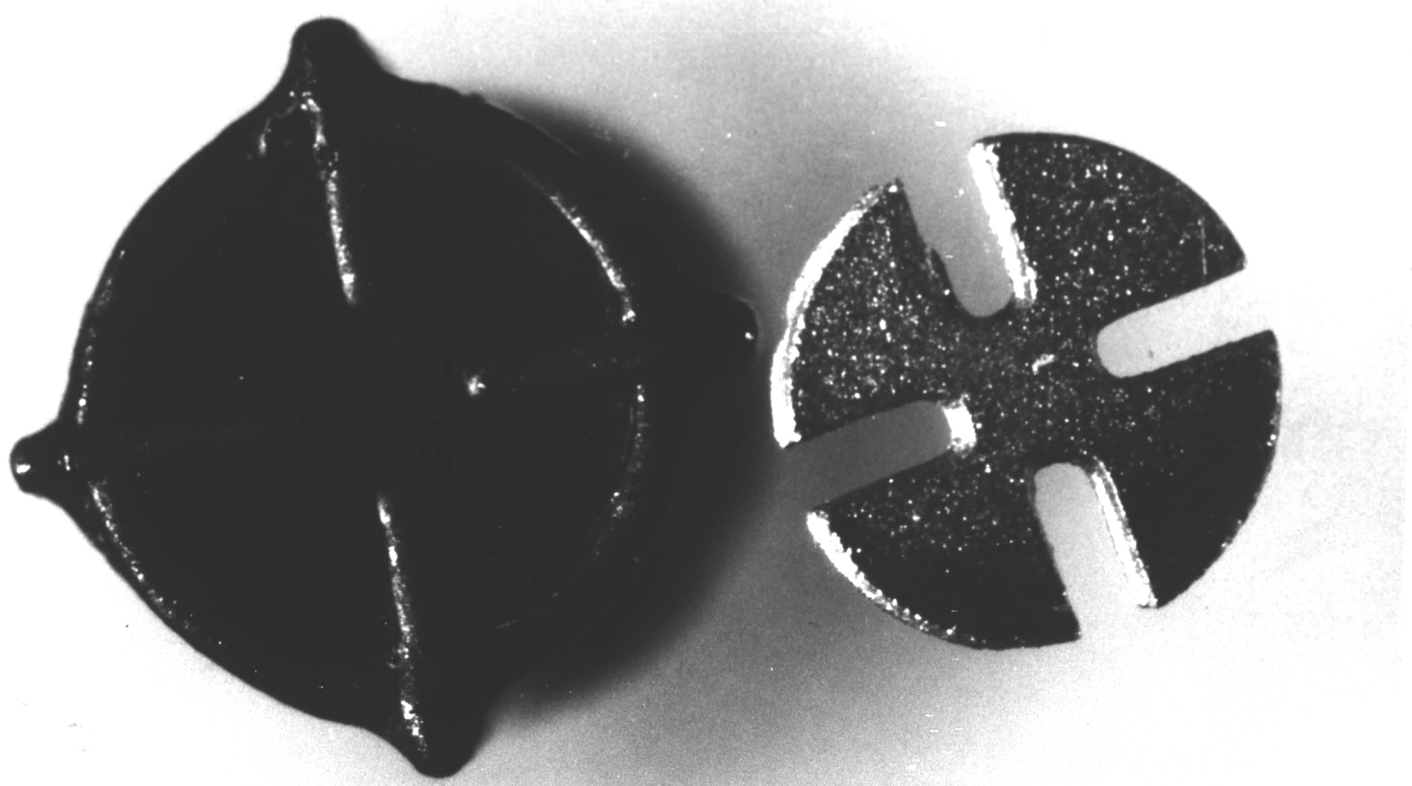

CLOVER LEAF TOOL AND CLOVER LEAF CUT SAMPLE

FIGURE 10

CIRCUIT SCHEMATIC FOR RESISTIVITY AND HALL MEASUREMENTS

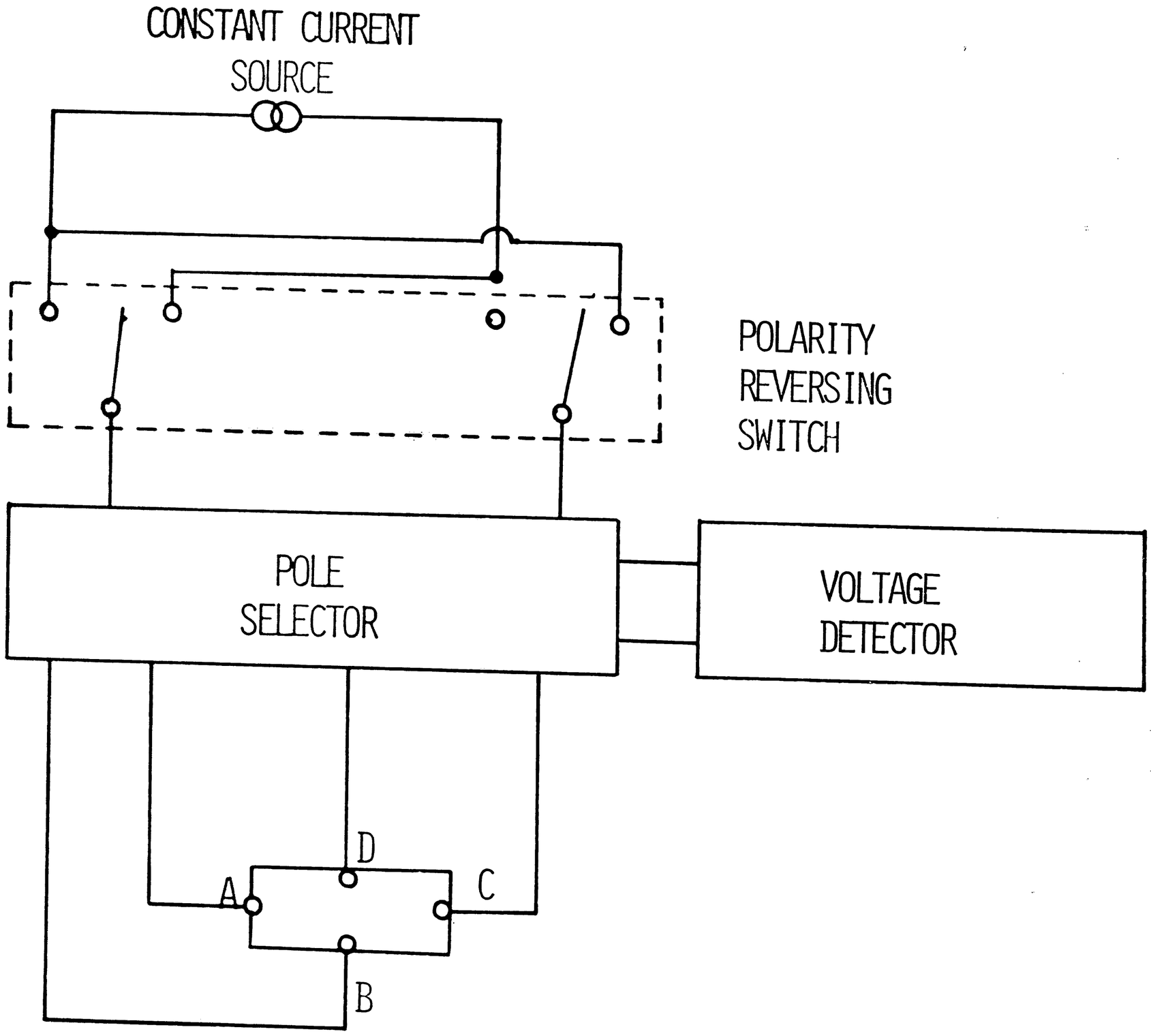

CIRCUIT SCHEMATIC FOR RESISTIVITY AND HALL MEASUREMENTS

FIGURE 11

OPTICAL EQUIPMENT FOR MEASURING THE PHOTOLUMINESCENT SPECTRA EMISSION AND THE PHOTOLUMINESCENT EFFICIENCY

OPTICAL EQUIPMENT FOR MEASURING THE PHOTOLUMINESCENT SPECTRA EMISSION AND THE PHOTOLUMINESCENT EFFICIENCY

FIGURE 12

PHOTOLUMINESCENT-SPECTRA MEASUREMENT ARRANGEMENT

PHOTOLUMINESCENT-SPECTRA MEASUREMENT ARRANGEMENT

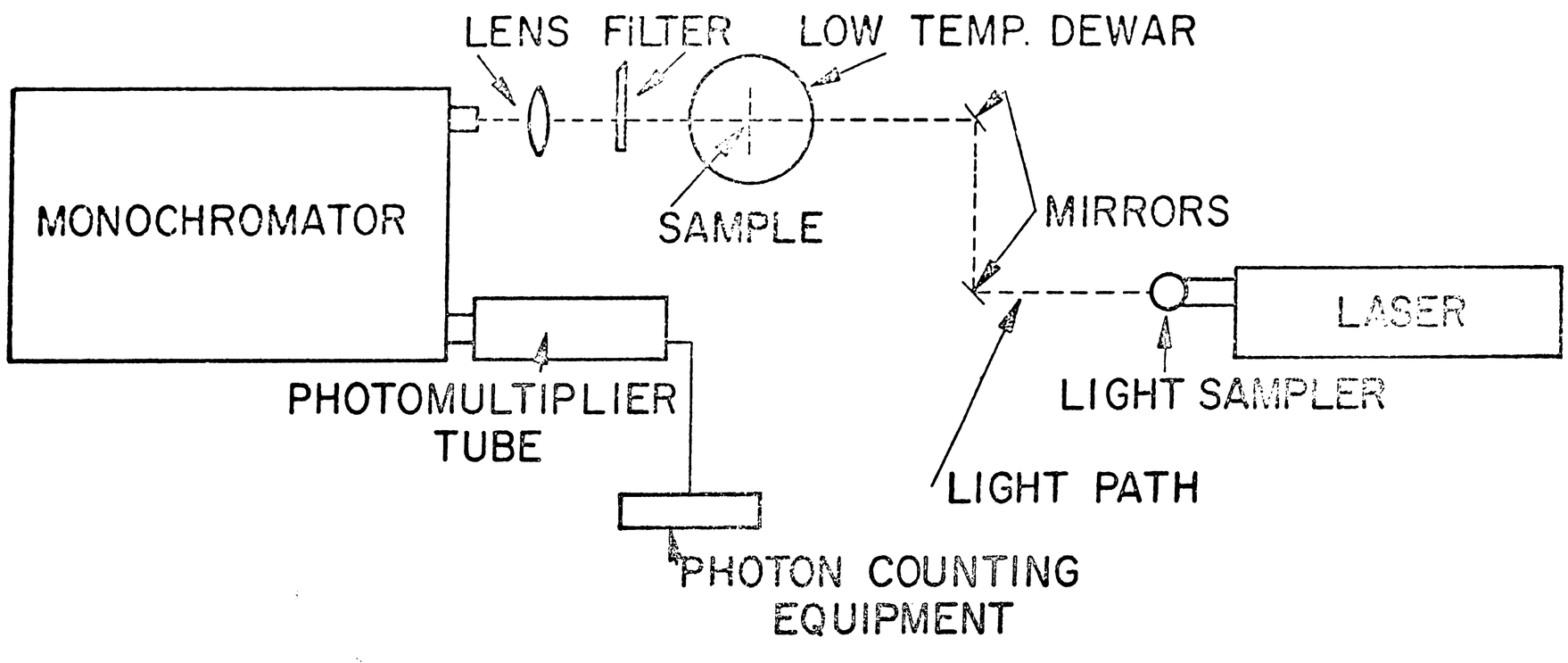

FIGURE 13

PHOTON-COUNTING SYSTEM

PHOTON-COUNTING SYSTEM

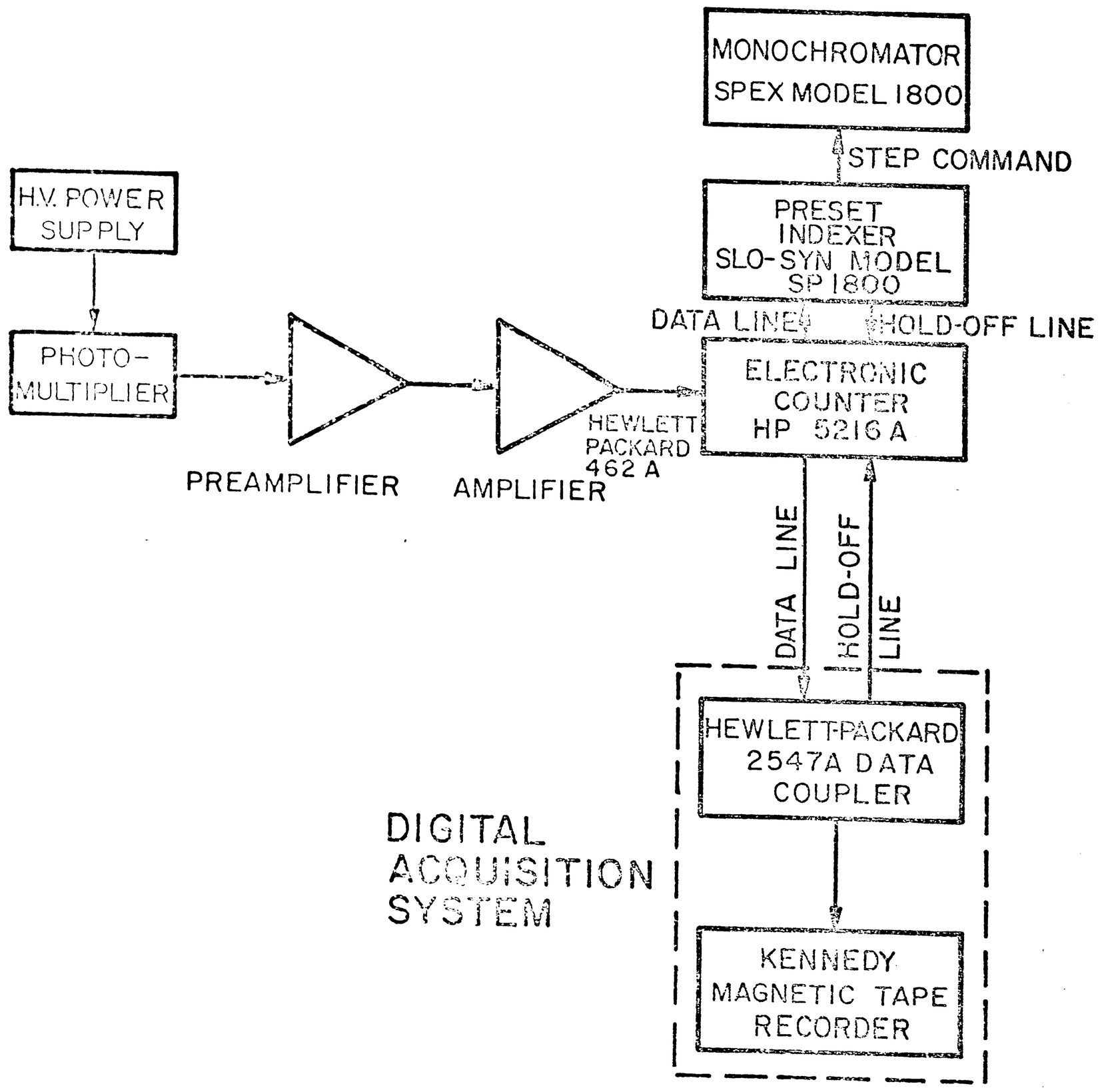

FIGURE 14

PHOTOLUMINESCENT EFFICIENCY TEST SET

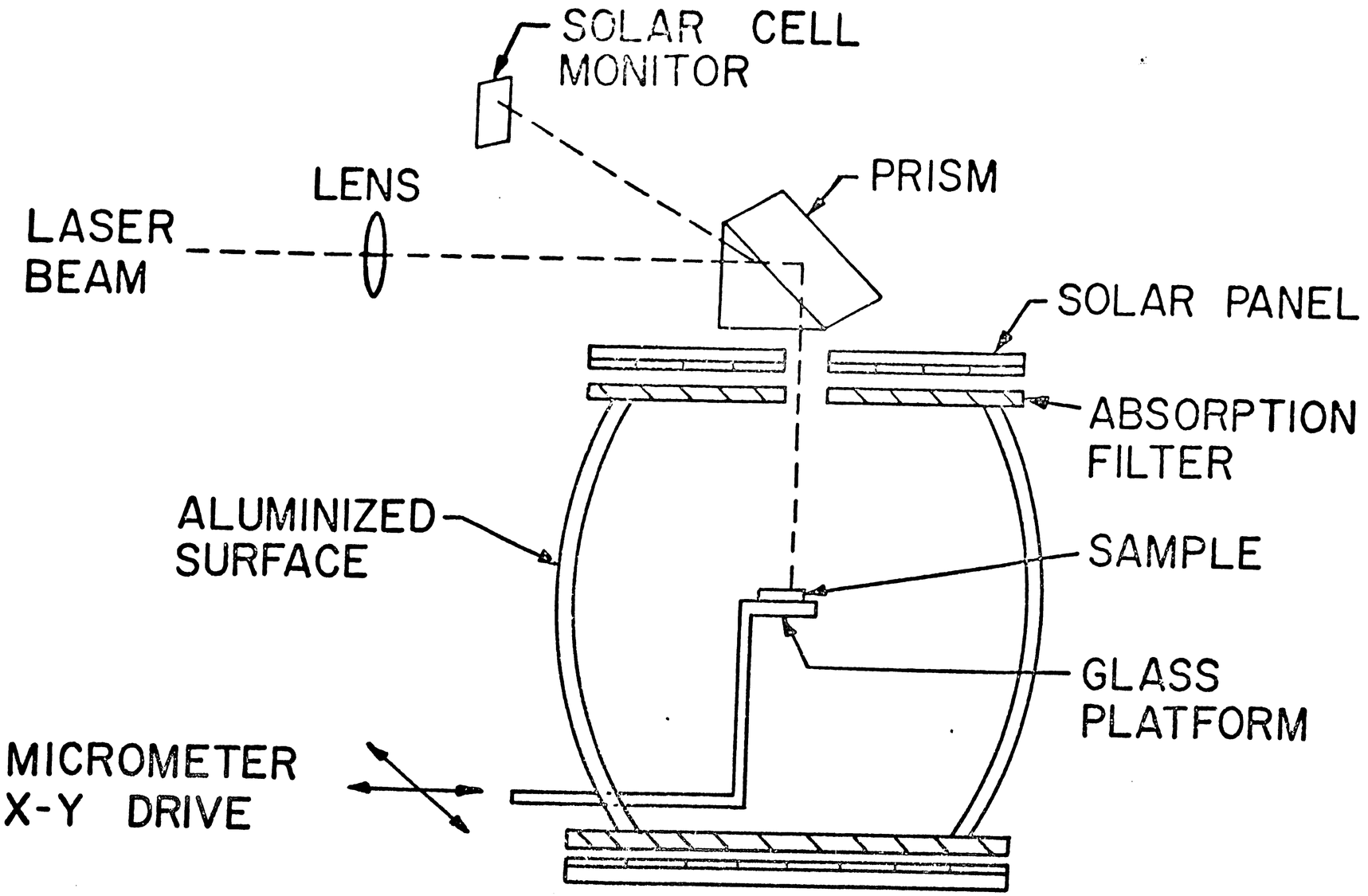

PHOTOLUMINESCENT EFFICIENCY TEST SET

FIGURE 15

EFFICIENCY VERSUS ANNEAL TIME FOR SAMPLE (H-140) ANNEALED AT 400°C

EFFICIENCY VERSUS ANNEAL TIME FOR
SAMPLE H-140 ANNEALED AT 400°C

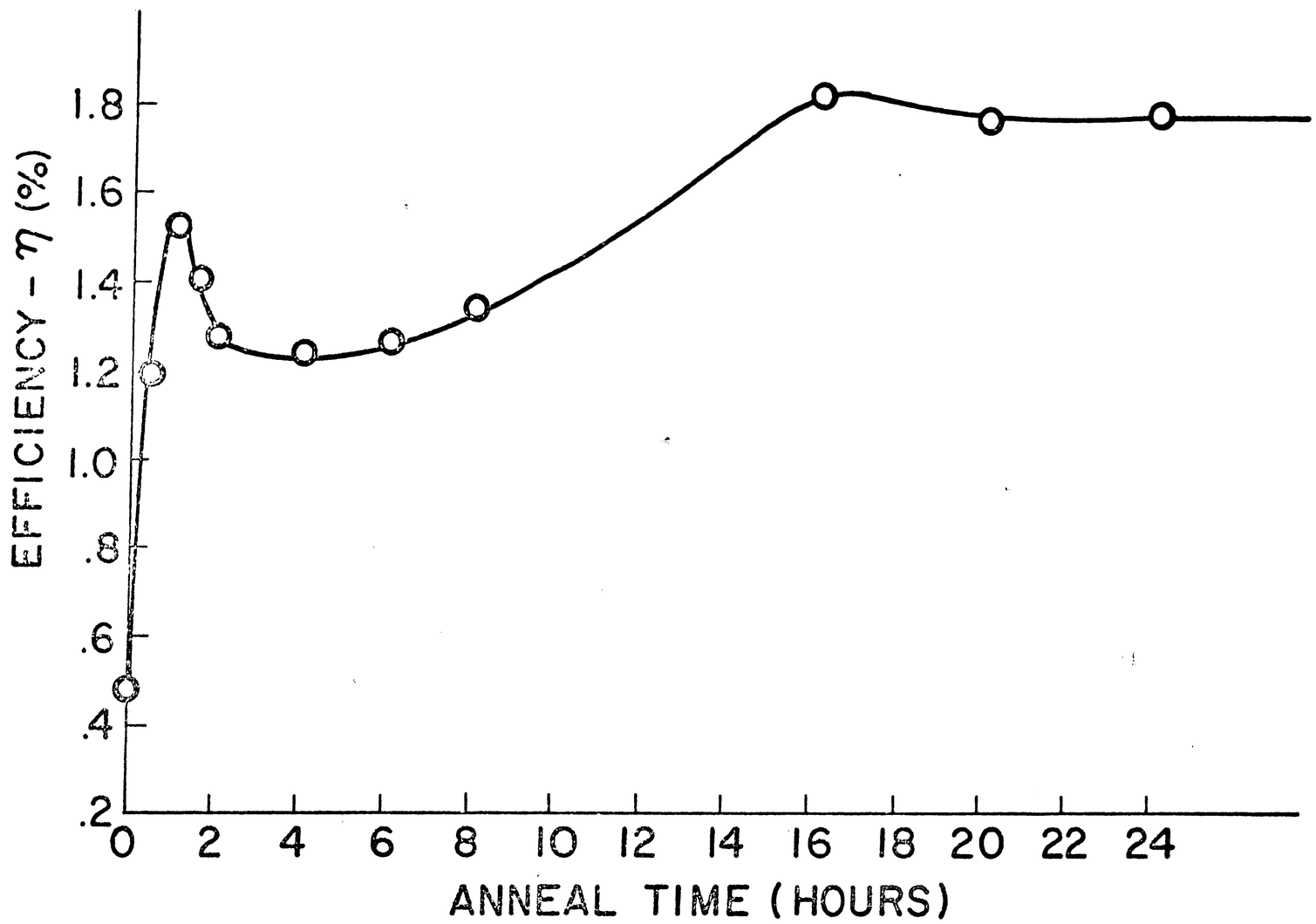

FIGURE 16

THE RELATIVE INTENSITY AS A FUNCTION OF WAVELENGTH FOR EMISSION OF SAMPLE (H-140) AT 77°K FOR THE "AS QUENCHED" CONDITION ($T=0$)

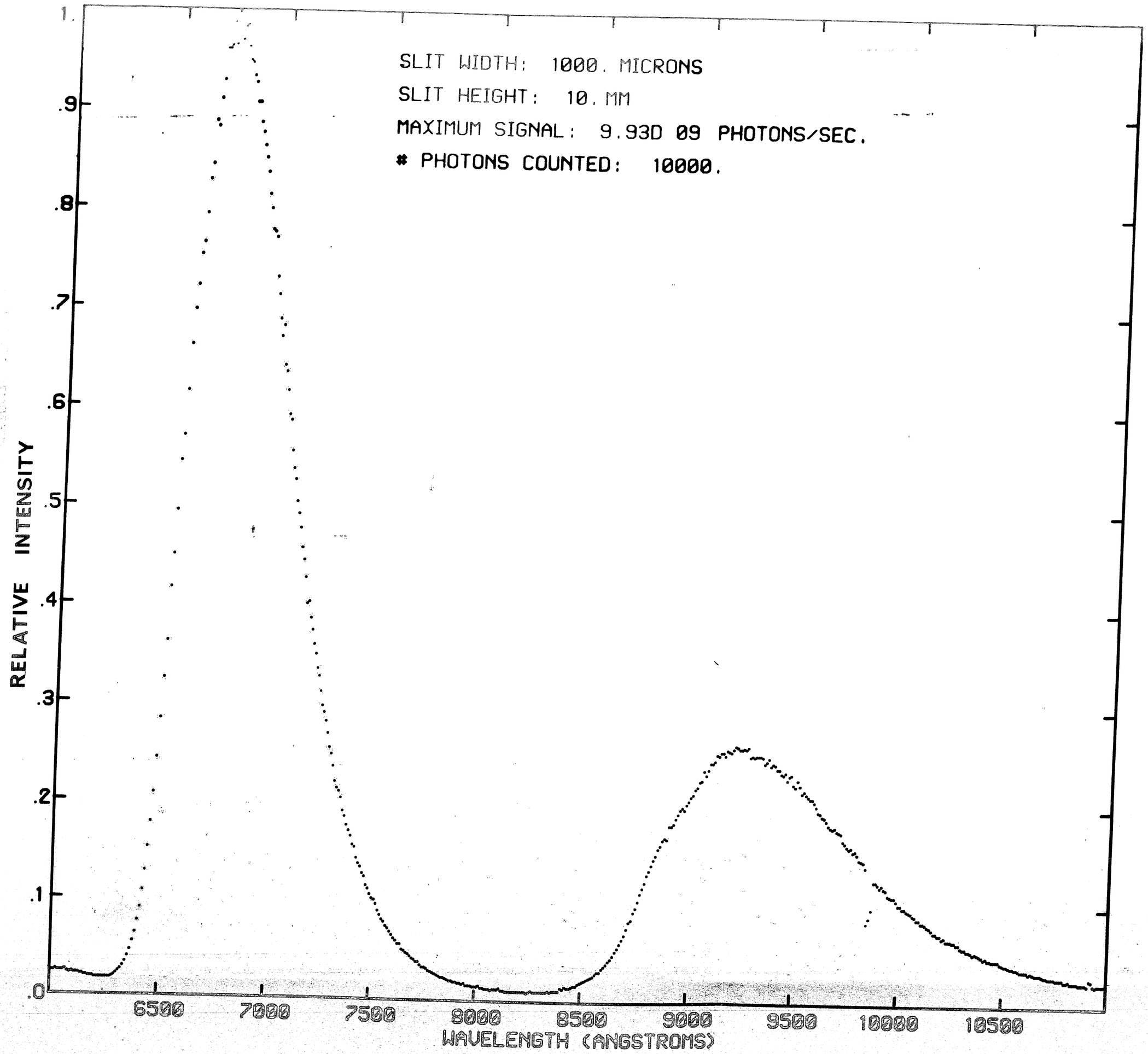

FIGURE 16 : EMISSION OF (H140); EXC. 4880 Å ; T=77 K;

FIGURE 17

THE RELATIVE INTENSITY AS A FUNCTION OF WAVELENGTH FOR EMISSION OF SAMPLE (H-140) AT 77°K FOR AN ANNEALING TIME OF 240 MINUTES AT 400°C

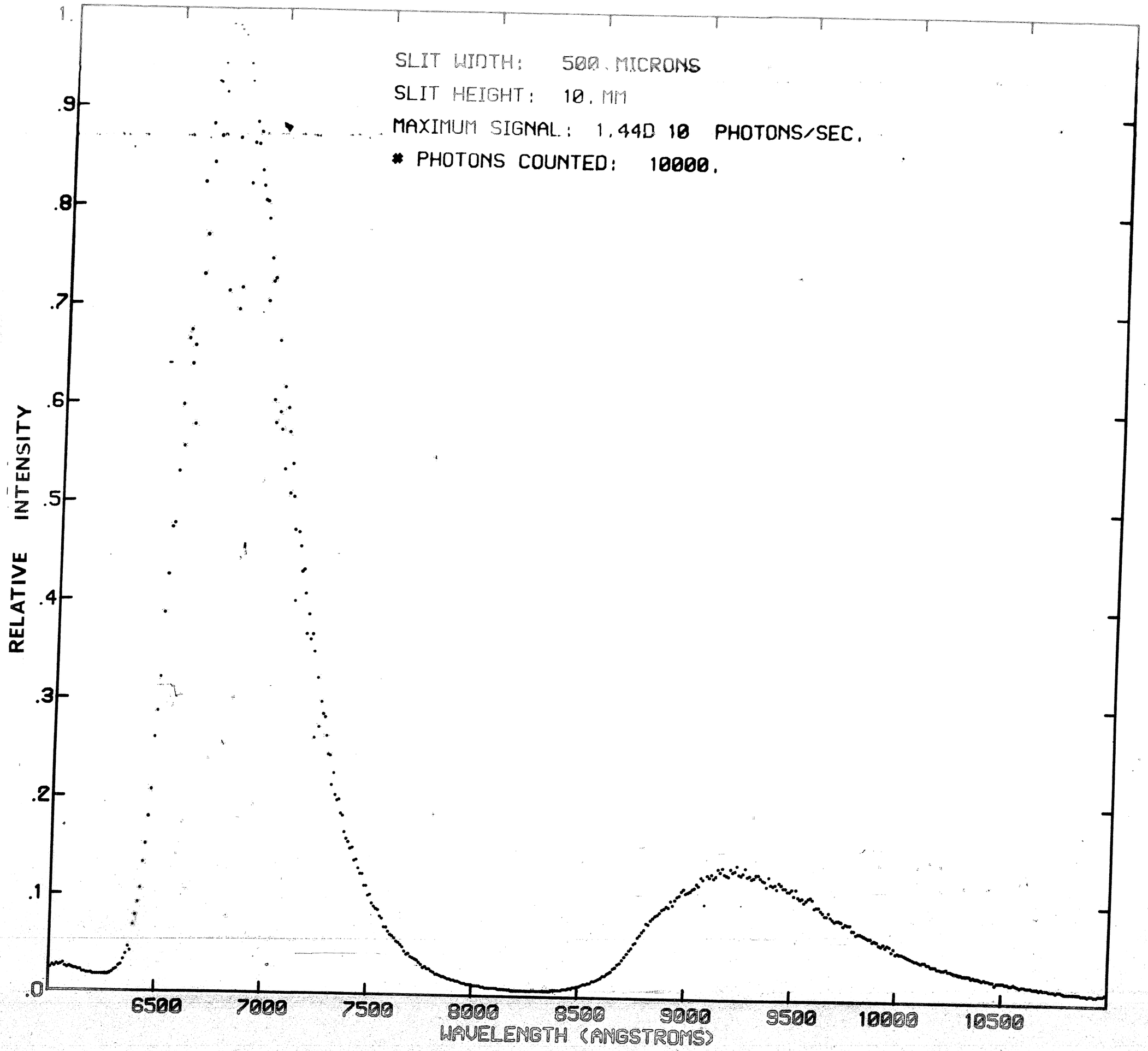

FIGURE 17 : EMISSION OF (H140); EXC. 4880 A ; T=77 K;
ANNEAL: 400 C; 240 MIN.

FIGURE 18

THE RELATIVE INTENSITY AS A FUNCTION OF WAVELENGTH FOR EMISSION OF SAMPLE (H-140) AT 77^{o}K FOR AN ANNEALING TIME OF 1200 MINUTES AT 400^{o}C

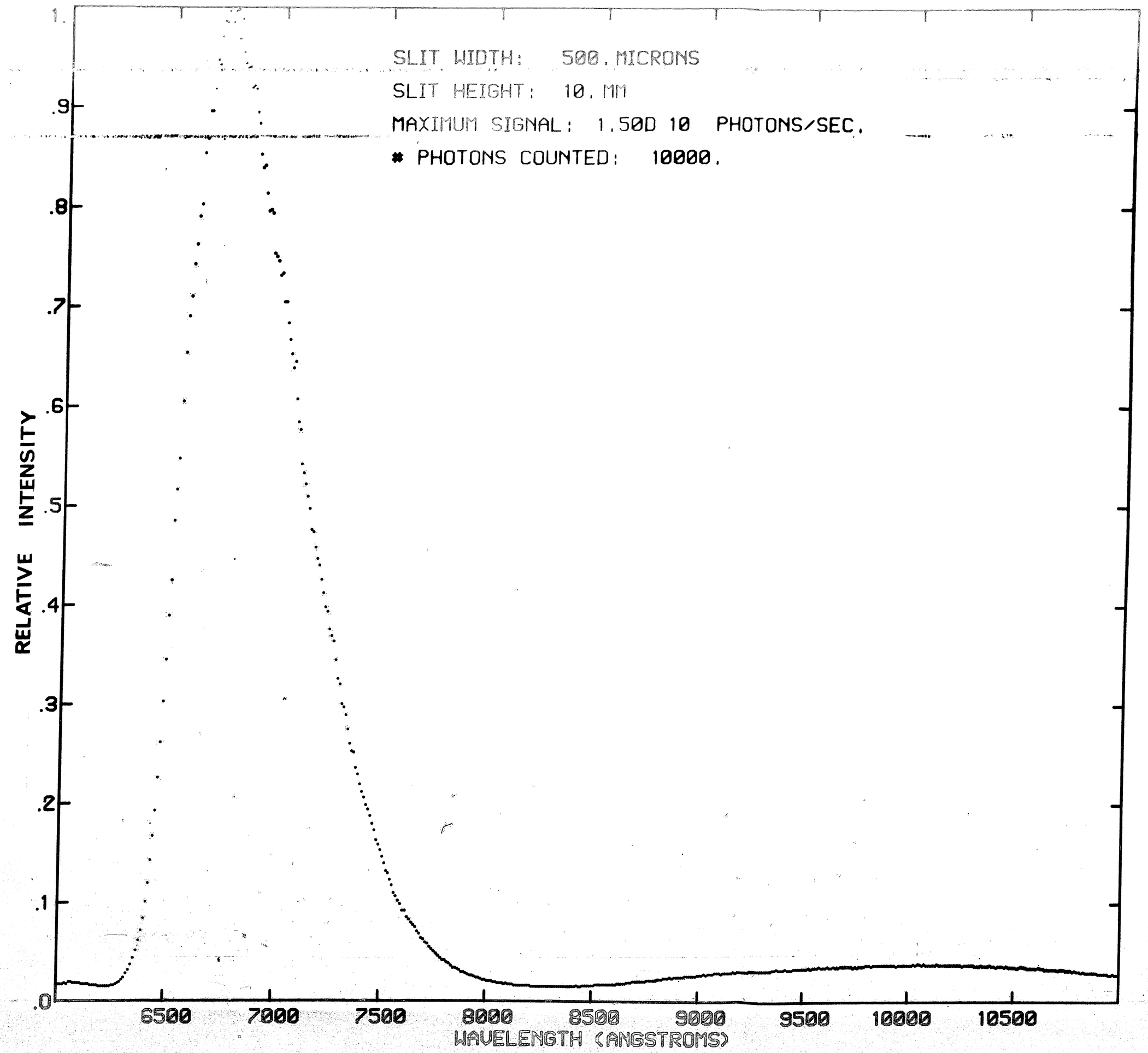

FIGURE 18: EMISSION OF (H140); EXC. 4880 A ; T=77 K;
ANNEAL: 400 C; 1200 MIN.

FIGURE 19

INTEGRATED RED TO INFRA-RED EMISSION RATIO VERSUS ANNEALING TIME FOR SAMPLE (H-140) ANNEALED AT 400^{o}C

INTEGRATED RED TO INFRA-RED EMISSION RATIO VERSUS ANNEALING TIME

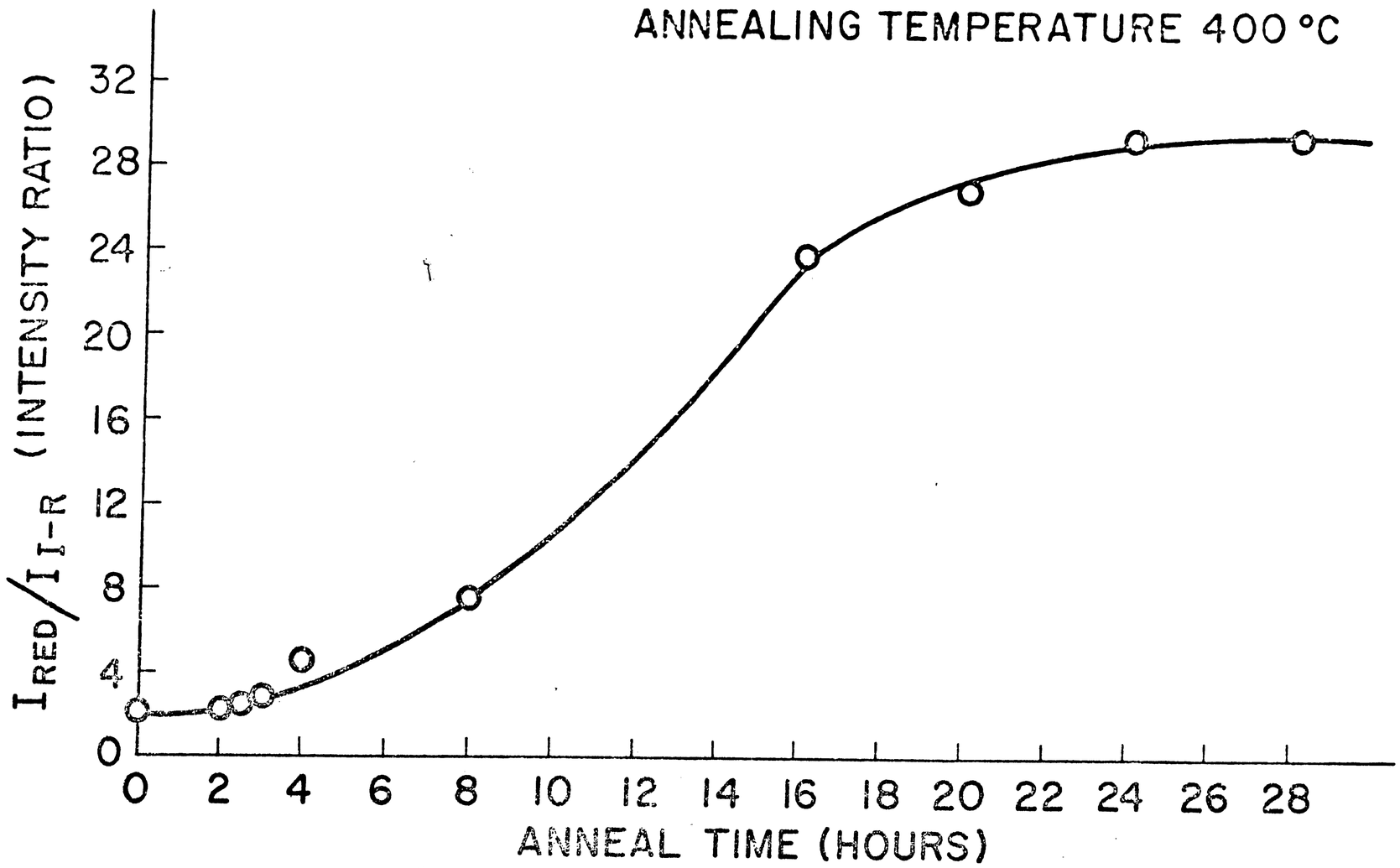

FIGURE 20

EFFICIENCY VERSUS ANNEAL TIME FOR SAMPLE (H-121) ANNEALED AT 600°C

EFFICIENCY VERSUS ANNEAL TIME FOR
SAMPLE H-121 ANNEALED AT 600°C

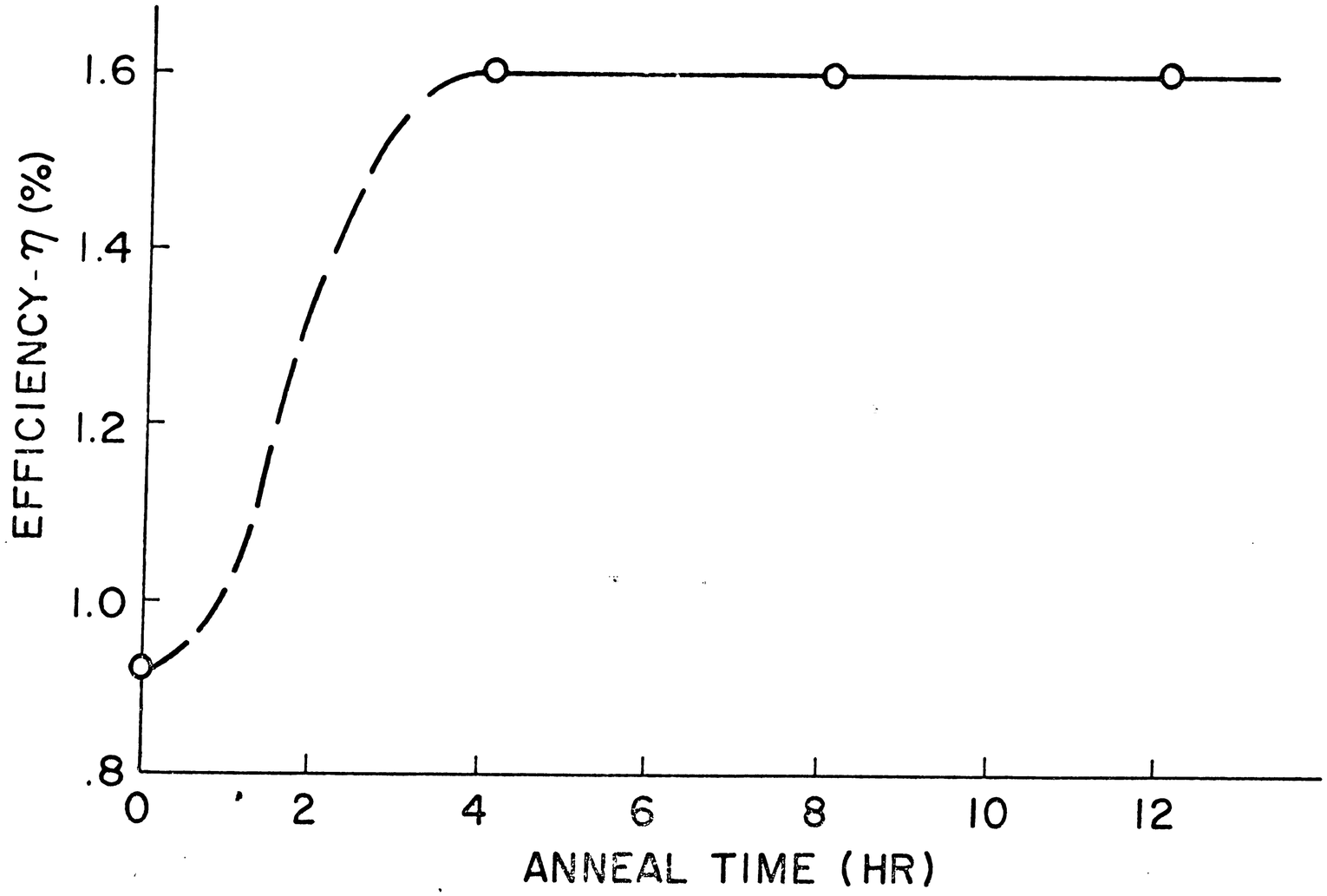

FIGURE 21

THE RELATIVE INTENSITY AS A FUNCTION OF WAVELENGTH FOR EMISSION OF SAMPLE (H-121) AT 77°K FOR AN ANNEALING TIME OF 240 MINUTES AT 600°C

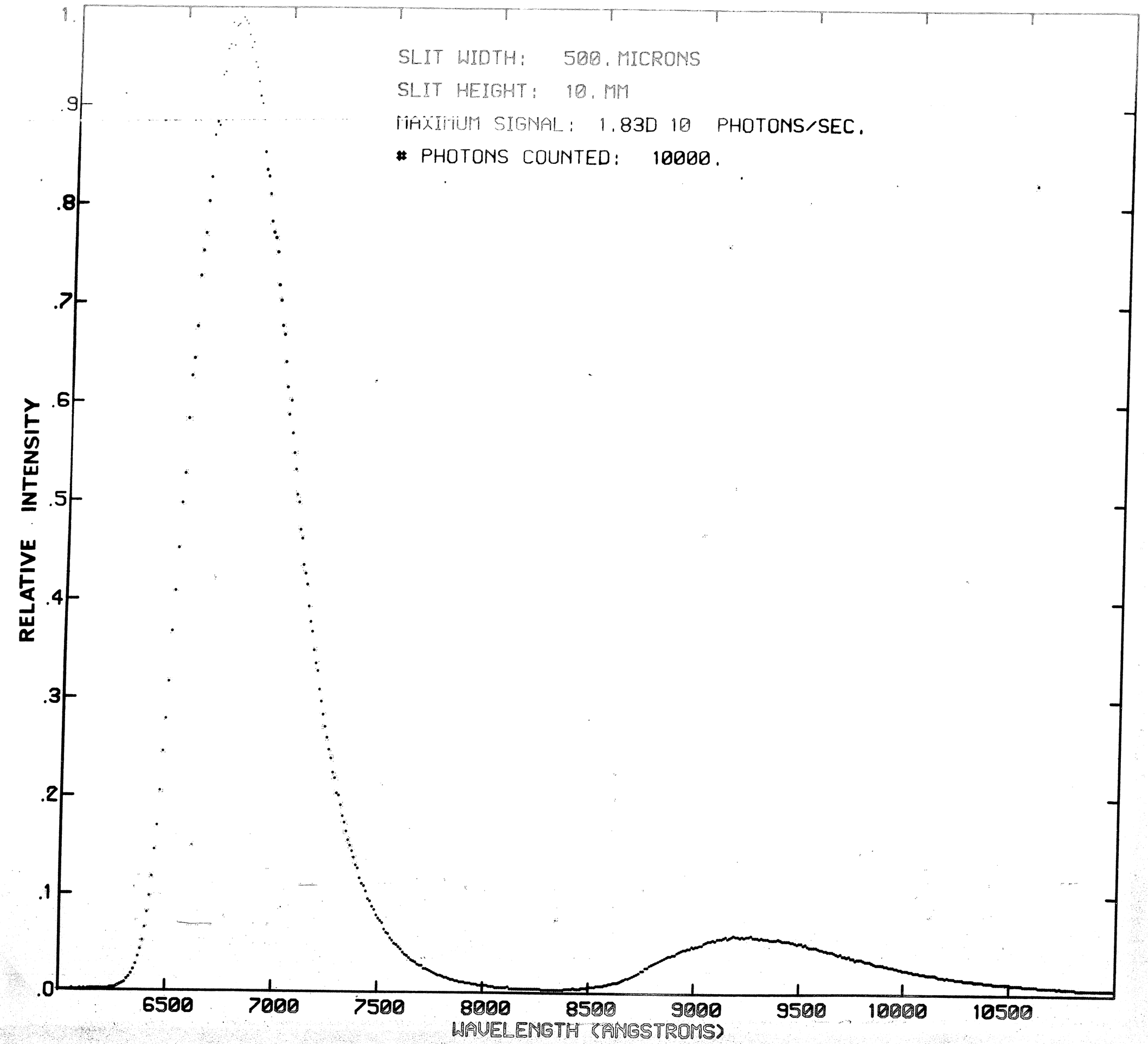

FIGURE 21 : EMISSION OF (H121); EXC. 4880 A ; T=77 K;
ANNEAL: 600 C; 240 MIN.

FIGURE 22

INTEGRATED RED TO INFRA-RED EMISSION RATIO VERSUS ANNEALING TIME FOR SAMPLE (H-121) ANNEALED AT 600^{o}C

INTEGRATED RED TO INFRA-RED
EMISSION RATIO VERSUS ANNEAL TIME

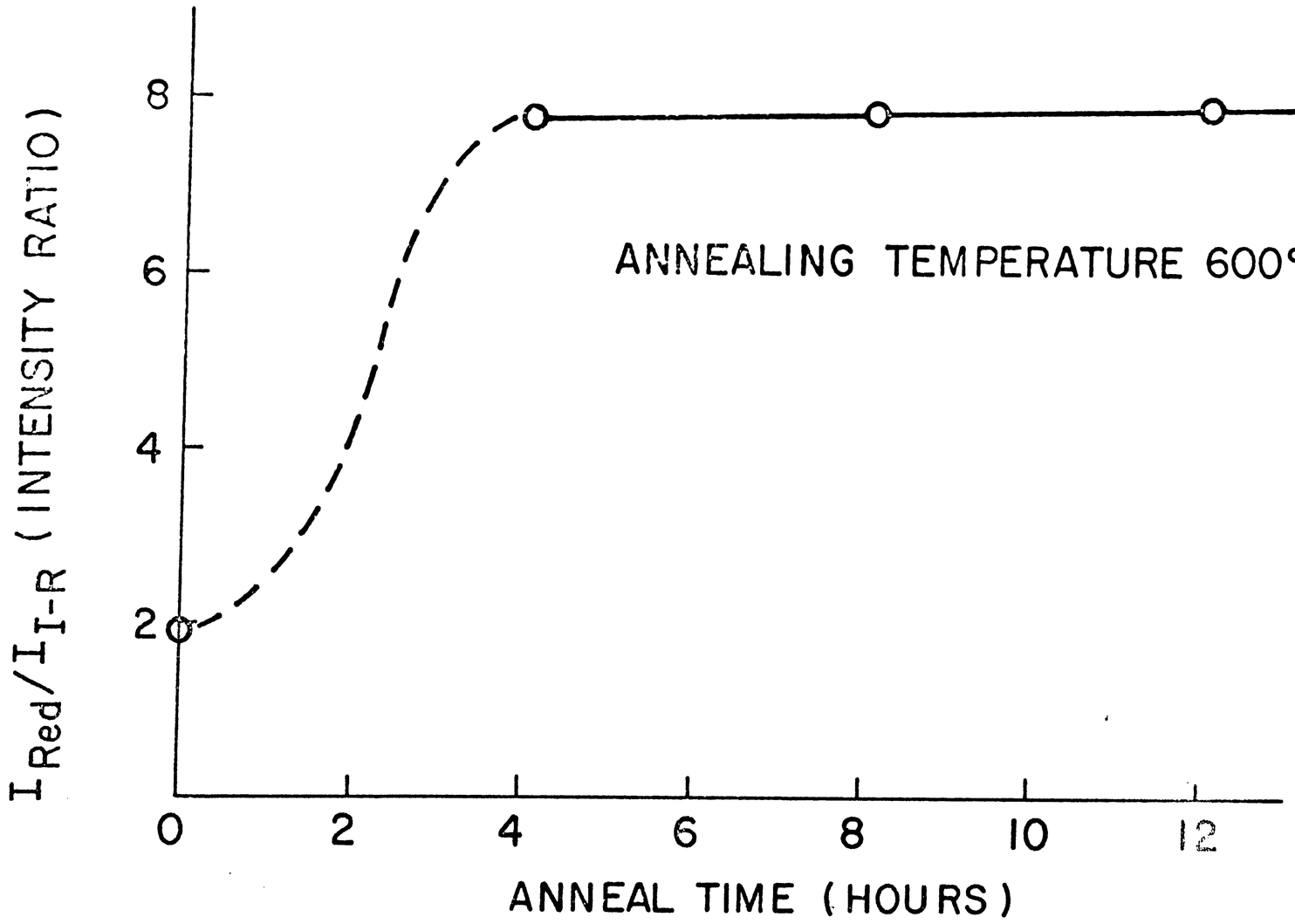

FIGURE 23

INTEGRATED RED TO INFRA-RED EMISSION RATIO (NORMALIZED) VERSUS ANNEALING TEMPERATURE

INTEGRATED RED TO INFRA-RED EMISSION RATIO (NORMALIZED) VERSUS ANNEALING TEMPERATURE

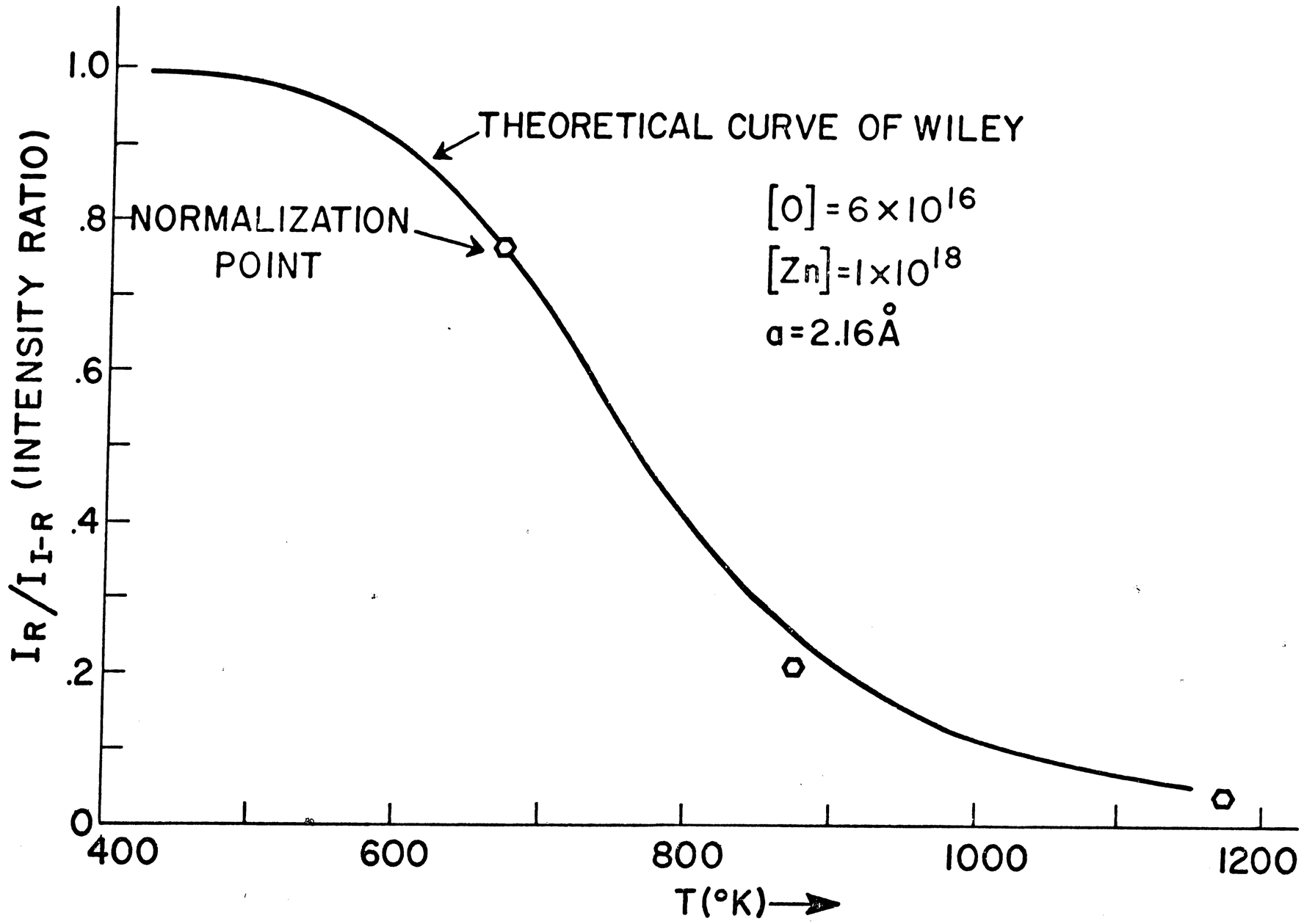

FIGURE 24

THE RELATIVE INTENSITY AS A FUNCTION OF WAVELENGTH FOR EMISSION OF SAMPLE (H-140) AT 77°K FOR THE "RESET" CONDITION

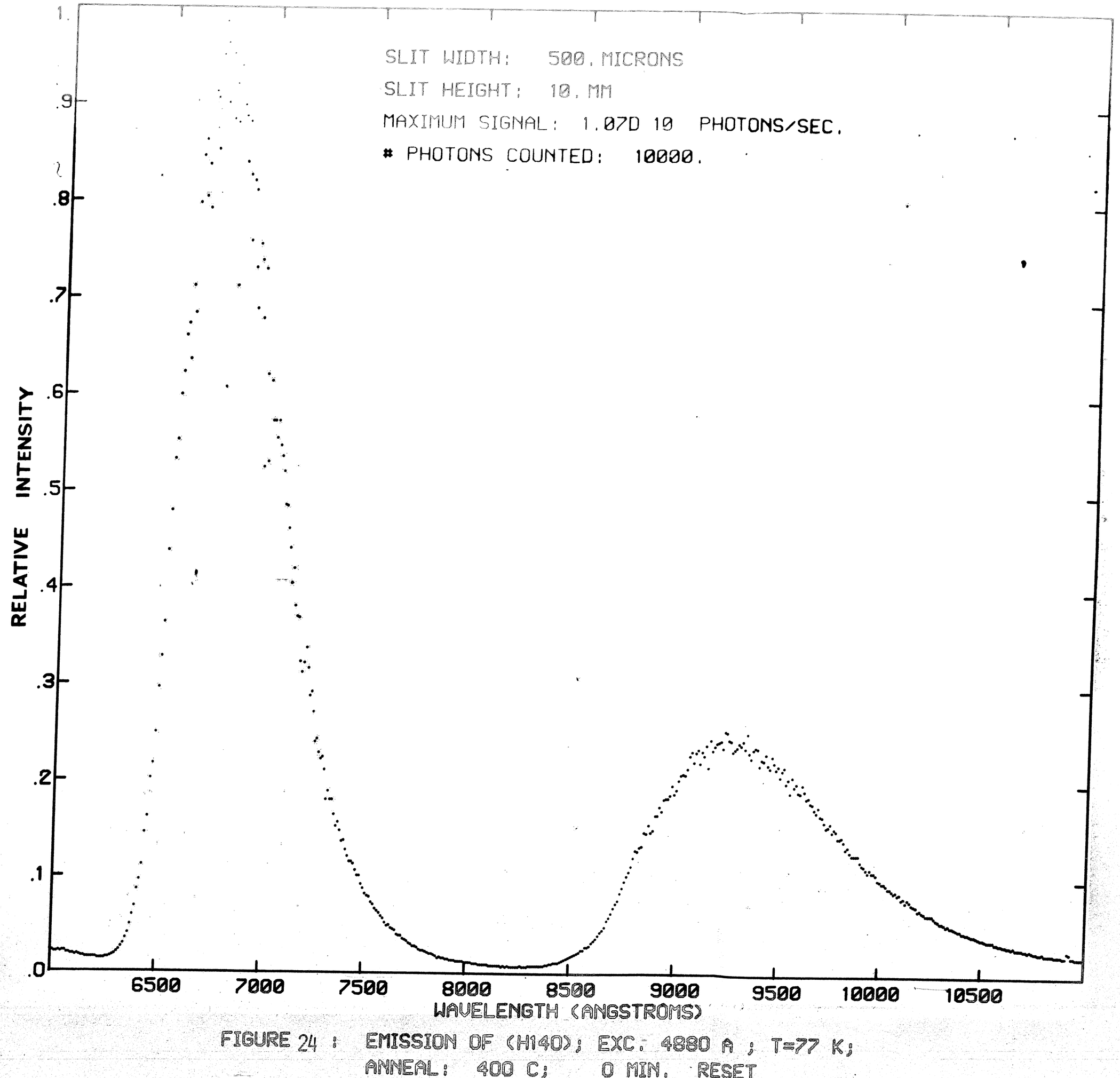

FIGURE 24 : EMISSION OF (H140); EXC. 4880 A ; T=77 K;
ANNEAL: 400 C; 0 MIN. RESET

APPENDIX A: Ampoule Preparation Sequence

1. Degrease with trichloroethylene (2 times).
2. Rinse with Methanol.
3. Rinse with D.I. water (2 times).
4. Rinse with HF (five minutes).
5. Rinse with D. I. water (10 times).
6. Rinse with Methanol (3 times).
7. Flow dry N_2 through while baking out with a torch (2-3 liter/min. for 3 minutes).
8. Cool with N_2 flow.

APPENDIX B: Cleaning Procedure for GaP Single Crystal Prior to R.F Sputtering

1. Gently swab sample with a cotton swab while the sample is immersed in methyl ethyl ketone (MEK). Use a petri dish lined with filter paper as a container for the MEK. Let the sample rest on the filter paper while swabbing; do not hold the sample with tweezers.
2. Quickly transfer the sample to a clean beaker containing methyl alcohol (MA).
3. Pour off the MA and rinse the sample with D.I. water.
4. Pour off the D.I. water; soak sample with solution of 1 part H_2SO_4, 1 part H_2O_2, and 3 parts H_2O for 2-3 minutes.
5. Pour off solution and rinse sample three times with D.I. water.
6. Pour off D.I. water and rinse sample with MA.
7. Pour off MA and rinse sample with chloroform.
8. Leave the sample in chloroform until sample is ready to be sputtered.

APPENDIX C: Photon Counting Theory

If a monochromatic beam of light of intensity H (watts/m^2) is incident on the photocathode of a photomultiplier, the power, P, intercepted is H times the photocathode area A. The number of photons striking the photocathode per unit time is

$$n_p = \frac{P}{h\nu} \qquad (1)$$

where $h\nu$ is the energy of each photon. If each photon produces N photoelectrons, the number of photoelectrons leaving the surface per unit time is

$$n_e = \eta\, n_p \qquad (2)$$

where η is the quantum efficiency. A fraction, κ, of the liberated photoelectrons are successful in reaching the first dynode. Each electron reaching the first dynode results in G electrons being collected at the anode, where G is the gain of the photomultiplier. The net result is that N_e electrons are collected per unit time, where N_e is given by

$$N_e = n_p \eta \kappa G \qquad (3)$$

The photomultiplier current produced by the light beam is

$$I = N_e q \qquad (4)$$

where $q = 1.6 \times 10^{19}$ coulombs is the charge of an electron.

In order to measure currents below about 10^{-10} amperes, special precautions must be taken to reduce leakage currents. In assuming a photomultiplier gain of $G = 10^6$, an anode current of 10^{-10} amperes results from $N_D = 625$ electrons per second reaching the first dynode from the follow relation,

$$N_D = I/(qG) \qquad (5)$$

Assuming $\eta = 0.2$ and $\kappa = 0.85$ as typical numbers, the number of intercepted photons per unit time is

$$n_p = N_D/(\eta\kappa) \simeq 3,670 \qquad (6)$$

Rather than measure current, it is possible to count the number of pulses produced at the anode per unit time and calculate incident power on the photomultiplier using the previously derived equations. Providing the pulses are of sufficient amplitude, an arbitrarily small number of pulses per second can be counted, and, consequently, a much lower light intensity can be detected by photon counting than by dc current detection techniques.

The above discussion, although correct, neglects the statistical nature of all physical processes. Each quantity in the previous equations is an average value since there are fluctuations in the rate of arrival of photons, in the number of photoelectrons generated by each photon, etc. Deviations in the number of photoelectrons generated per photon, etc., result in deviations in the number of electrons N_e collected at the anode for each incident photon. Since each group of collected electrons produces a voltage pulse across the photomultiplier load resistor, R_L, the amplitude of the signal pulse fluctuates in proportion to the fluctuations in N_e. A further consideration is that electrons thermally emitted by the photocathode are indistinguishable from those created by incident light. In dc detection techniques, the minimum detectable signal is approximately equal to the current produced by the thermally emitted electrons, i.e., the "dark current."

In photon counting, signal-to-noise ratios are determined by statistics. If N_p photons are counted in a time interval τ, statistical analysis shows that the probable (rms) deviation in the average value, $\bar{N}_p$, is $(\bar{N}_p)^{1/2}$. Inasmuch as this deviation constitutes noise, the signal-to-noise ratio -- neglecting pulses caused by thermionic-electron -- is:

$$S/N = \frac{\bar{N}_p}{(\bar{N}_p)^{1/2}} = (\bar{N}_p)^{1/2} \qquad (7)$$

From this result it is evident that in order to improve the detection system S/N ratio when detecting light by photon counting, longer time intervals are required in order to make N_p larger.

The above analysis is somewhat complicated by our inability to distinguish between electrons which are thermally emitted at the photocathode and those which are liberated by incident photons. For a given time interval, let $\bar{N}_d$ be the average number of "dark" counts which are caused by thermally emitted electrons when there is definitely no incident light on the photocathode. If, now, N_s signal photons are counted for the same length of time, τ, the total number of counts will be $N_s + N_d$. The signal to noise will be

$$S/N = \frac{(N_s + N_d) - N_d}{(N_s + 2N_d)^{1/2}} = \frac{N_s}{(N_s + 2N_d)^{1/2}} \qquad (8)$$

The factor of 2 in the denominator arises because of deviation of $(N_d)^{1/2}$ is contributed when determining N_d alone and again when determining $N_s + N_d$, whereas the deviation in N_s is only contributed while determining $N_s + N_d$.

Instead of writing S/N in terms of N_s and N_d, it is convenient to write it in terms of the corresponding count rates, r_s and r_d. It can be seen that $N_d = r_d \tau$ and $N_s = r_s \tau$, so that

$$S/N = \frac{r_s \tau}{(r_s \tau + 2 r_d \tau)} \; 1/2 = \frac{r_s \tau 1/2}{(r_s + 2 r_d)} \; 1/2 \qquad (9)$$

Letting $N = N_s + N_d$, then

$$\tau = N/(r_s + r_d) \qquad (10)$$

Substituting for τ,

$$S/N = \frac{r_s (N)^{1/2}}{[(r_s + r_d)(r_s + 2 r_d)]} \; 1/2 \qquad (11)$$

$$= \frac{(N)^{1/2}}{\left[\left(1 + \frac{2 r_d}{r_s}\right)\left(1 + \frac{r_d}{r_s}\right)\right]} \; 1/2$$

This result indicates that for a given ratio, (r_d/r_s), the S/N ratio is determined by the total number of signal-plus-dark counts. In practice, r_d was determined by counting dark pulses over an extended period of time (15 minutes) so that the rms deviation in determining r_d was much less than that which results in measuring r_s and r_d. Therefore, the factor of 2 which multiplied r_d in eq. 11 should be replaced by unity and the signal to noise ratio can be written,

$$S/N = \frac{N^{1/2}}{1 + rd/rs} \qquad (12)$$

BIBLIOGRAPHY

1. Thomas, D. G., "Electroluminescence," Physics Today, V. 21, No. 2, p. 43, (February, 1968)

2. Lossev, O. W., Telegrafia i Telefonia, V. 18, p. 61, (1923)

3. Destriau, G., "Analytical Study of the Conditions of Excitation of the Phenomena of Electro-Photoluminescence," Journal de Chimique Physique, V. 34, p. 462, (1937)

4. Haynes, J. R., and Briggs, H. B., "Radiation Produced in Germanium and Silicon by Electron-Hole Recombination," Physical Review, V. 86, p. 647, (1952)

5. Keyes, R. J., and Quiest, T. M., "Recombination Radiation Emitted by Gallium Arsenide," Proceeding Institute of Radio Engineers (USA), V. 50, No. 8, p. 1822, (August, 1962)

6. Holonyak, N. Jr., and Bevacqua, S. F., "Coherent (Visible) Light Emission from $Ga(As_{1-x}P_x)$ Junctions," Applied Physics Letters, V. 1, No. 4, p. 82, (December, 1962)

7. Grimmeis, H. G., and Scholz, H., "Efficiency of Recombination Radiation in GaP," Physics Letters, (Netherlands) V. 8, No. 4, p. 233, (May, 1964)

8. Dean, P. J., Luminescence of Inorganic Solids, Academic Press, New York, (1966), p. 119, Ed. Paul Goldberg; Gershenzen, M., Luminescence of Inorganic Solids, Academic Press, New York, (1966), p. 203, Ed. Paul Goldberg

9. Gershenzen, M., Semiconductors & Semimetals, Academic Press, New York, (1966), p. 289, Ed. R. K. Willardson and A. C. Beer

10. Gershenzen, M., Logan, R. A., and Nelson, D. F., "Electrical and Electroluminescent Properties of Gallium Phosphide Diffused P-N Junctions," Physical Review, V. 149, No. 2, p. 580, (September, 1966)

11. Dean, P. J., Henry, C. H., and Frosch, C. J., "Infrared Donor-Acceptor Pair Spectra Involving the Deep Oxygen Donor in Gallium Phosphide," Physical Review, V.168, No. 3, p. 812, (April, 1968)

12. Hall, R. N., "Electron-hole Recombination in Germanium," Physical Review, V. 87, p. 387, (July, 1952)

13. Shockley, W., and Read, W. T. Jr., "Statistics of the Recombinations of Holes and Electrons," Physical Review, V. 87, p. 835, (September, 1952)

14. Lorenz, M. R., "Visible Light from Semiconductors," Science, V. 159, No. 3822, p. 1419, (March, 1968)

15. Lorenz, M. R., "The Generation of Visible Light from P-N Junctions in Semiconductors," Transactions of the Metallurgical Society of AIME, V. 245, p. 539, March, 1969)

16. Gershenzen, M., Trumbore, F. A., Mikulyok, R. M., and Kowalchik, M., "Radiative Recombination between Deep Donor-Acceptor Pairs in GaP," Journal of Applied Physics, V. 36, No. 5, p. 1528, (1965)

17. Gershenzen, M., Trumbore, F. A., Mikulyok, R. M., and Kowalchik, M., "Evidence for Radiative Recombination between Deep Donor-Acceptor Pairs in GaP at Room Temperature," Journal of Applied Physics, V. 37, No. 2, p. 483, (February, 1966)

18. Nelson, D. F., and Rodgers, K. F., "Time Decay Characteristics of a Deep Donor-Shallow-Pair Band in Gallium Phosphide," Physical Review, V. 140, No. 5A, p. A 1667, (November, 1965)

19. Morgan, T. N., Welber, B., Bhargava, R. N., Optical Properties of Cd-O & Zn-O Complexes in GaP," Physical Review, V. 166, No. 3, p. 751, (February, 1968)

20. Henry, C. H., Dean, P. J., "New Red Pair Luminescence from GaP," Physical Review, V. 166, No. 3, p. 754 (February, 1968)

21. Cuthbert, J. D., Henry, C. H., and Dean, P. J., "Temperature-Dependent Radiative Recombination Mechanisms in GaP (Zn,O) & GaP (Cd,O)," Physical Review, V. 170, No. 3, p.739, (June, 1968)

22. Logan, R. A., White, H. G., and Wiegmann, W., "Efficient Green Electroluminescence in Nitrogen-Doped GaP p-n Junctions," Applied Physics Letters, V. 13, No. 4, p. 139, (August, 1968)

23. Logan, R. A., White, H. G., and Trumbore, F. A., "P-N Junctions in GaP with External Electroluminescence Efficiency 2% at 25°C," Applied Physics Letters, V. 10, No. 7, p. 206, (April, 1967)

24. Onton, A., and Lorenz, M. R., "Dependence of Radiative Efficiency in GaP Diodes on Heat Treatment," Applied Physics Letters, V. 12, No. 4, p. 115, February, 1968)

25. Maeda, Keije, "Temperature Dependence of Pair Band Luminescence in GaP," Physical Chemical Solids, V. 26, p. 595, Pergamon Press, (1965)

26. Toyama, M., Kasami, , A., Naito, M., and Maeda, K., "Effect of Heat Treatment of Diffused Gallium Phosphide Electroluminescent Diodes," Transaction of the Metallurgical Society of AIME,

V. 245, p. 551, (March, 1969)

27. Maeda, K., Kasami, A., Toyama, M., and Wakamatsu, N., "Minority Carrier Lifetime in GaP Electroluminescent Diodes," Japanese Journal of Applied Physics, V. 8, No. 1, p. 65, (January, 1969)

28. Trumbore, F. A., Private conversation on September 25, 1969, (BTL)

29. Thurmond, C. D., "Phase Equilibria in the GaAs and the GaP Systems," Journal of Physics and Chemistry of Solids, V. 26, p. 789, Pergamon Press, (1965)

30. Trumbore, F. A., Private conversation on March 17, 1970, (BTL)

31. Ketchow, D. R., Private conversation on January 12, 1970, (BTL)

32. van der Pauw, L. J., "A Method of Measuring Specific Resistivity and Hall Effect of Discs of Arbitrary Shapes," Philips Research Report, V. 13, No. 1, p. 1, (February, 1958)

33. Hindle, P. H., and Ibbett, R. N., "A Digitization System for a Scanning Spectrometer," Journal of Scientific Instruments, V. 43, p. 209, (1966)

34. Hertz, L. M., Solid State Lamp Manual 3-8270, General Electric, p. 29, (1968)

35. Diguet, D., "Electrical Properties of Bulk Solution Grown GaP and GaAs Crystals," Solid State Electronics, V. 13, p. 37 Pergamon Press, (1970)

36. Wiley, J. D., to be published

37. Lidiard, A. B., "Ionic Conductivity of Impure Polar Crystals," Physical Review, V. 94, No. 1, p. 29, (April, 1954)

38. Fowler, R. H., Guggenheim, E. A., Statistical Thermodynamics, Cambridge, (1965) p. 390

39. Foster, L. M., and Scardefield, J., "Oxygen Doping of Solution Grown GaP," Journal of Electrochemical Society: Solid State Science, V. 116, p.494, (1969)

40. Luther, L., to be published

VITA

Donald Leroy Hughes was born December 18, 1940 in Ludlow, Missouri.

Mr. Hughes was graduated from Westport High School in Kansas City, Missouri in June 1958. From 1958 to 1960 he attended Brigham Young University where he majored in Electrical Engineering. After serving as a missionary for the Church of Jesus Christ of Latter Day Saints for three years in France, he returned to Brigham Young University and was graduated from a five year engineering program with a Bachelor of Engineering Science in Electrical Engineering in August, 1966.

Before graduation, in 1963, Mr. Hughes, married Betty Jean Greenway. The summer of 1965, Mr. Hughes worked for Western Electric in Kansas City in the semiconductor field. After graduation, he returned to Western Electric at Kansas City as a Product Engineer with responsibilities for testing transistors on a production line. Since 1968, he has been a Lehigh Master's candidate at the Corporate Education Center (Western Electric - Princeton) where he has been working on the effects of annealing on GaP light emitting diodes.

Mr. Hughes is a member of Tau Beta Pi and the Institute of Electrical and Electronic Engineers.